THE USE OF BORON-DOPED DIAMOND FILM ELECTRODES FOR THE OXIDATIVE DEGRADATION OF PERFLUOROOCTANE SULFONATE AND TRICHLOROETHYLENE

BY

KIMBERLY ELLEN CARTER

A Dissertation Submitted to the Faculty of the

DEPARTMENT OF CHEMICAL AND ENVIRONMENTAL ENGINEERING

In Partial Fulfillment of the Requirements
For the Degree of

DOCTOR OF PHILOSOPHY
WITH A MAJOR IN ENVIRONMENTAL ENGINEERING

In the Graduate College

THE UNIVERSITY OF ARIZONA

2009

THE UNIVERSITY OF ARIZONA
GRADUATE COLLEGE

As members of the Dissertation Committee, we certify that we have read the dissertation prepared by Kimberly Ellen Carter
entitled The Use of Boron-Doped Diamond Film Electrodes for the Oxidative Degradation of Two Organic Compounds in Aqueous Solutions: Pefluorooctane Sulfonate (PFOS) and Trichloroethene (TCE)
and recommend that it be accepted as fulfilling the dissertation requirement for the Degree of Doctor of Philosophy

_____ Date: April 8, 2009
James Farrell

_____ Date: April 8, 2009
Wendell Ela

_____ Date: April 8, 2009
Eduardo Saez

_____ Date: April 8, 2009
Reyes Sierra

Final approval and acceptance of this dissertation is contingent upon the candidate's submission of the final copies of the dissertation to the Graduate College.

I hereby certify that I have read this dissertation prepared under my direction and recommend that it be accepted as fulfilling the dissertation requirement.

_____ Date: April 8, 2009
Dissertation Director: James Farrell

STATEMENT BY AUTHOR

This dissertation has been submitted in partial fulfillment of requirements for an advanced degree at the University of Arizona and is deposited in the University Library to be made available to borrowers under rules of the Library.

Brief quotations from this dissertation are allowable without special permission, provided that accurate acknowledgement of source is made. Requests for permission for extended quotation from or reproduction of this manuscript in whole or in part may be granted by the head of the major department or the Dean of the Graduate College when in his or her judgment the proposed use of the material is in the interests of scholarship. In all other instances, however, permission must be obtained from the author.

SIGNED: Kimberly E. Carter

ACKNOWLEDGEMENTS

Many people helped me through the research and writing of this dissertation. I would first like to thank my advisor Dr. James Farrell. Dr. Farrell gave me the opportunity to work on this research and in doing so I gained a greater knowledge than I would have ever gained elsewhere. I am very grateful for his guidance, understanding and support through my years here.

I would like to thank Dr. Ela, Dr. Saez, and Dr. Sierra for being on my committee. Thank you for answering my questions over the years and helping me understand what I did not.

I would like to thank my colleagues for their help with my research. Lily Liao and her analytical expertise helped to develop my skills in the lab. I would like to thank my friends for always being there through all the good and bad.

I would like to thank my family for their love. My parents who have given me the strength and guidance to strive for what I wanted out of life and my career. Finally, I would like to thank Marco, my love and best friend, for giving me his patience, support, understanding, and love.

TABLE OF CONTENTS

TABLE OF CONTENTS – Continued

LIST OF FIGURES

LIST OF FIGURES – Continued

LIST OF FIGURES – Continued

LIST OF TABLES

ABSTRACT

The current treatment of water contaminated with organic compounds includes adsorption, air stripping, and advanced oxidation processes. These methods large quantities of water and require excessive energy and time. A novel treatment process of concentrating and then electrochemically oxidizing compound would be a more feasible practice. This research investigated the oxidative destruction of perfluorooctane sulfonate (PFOS), perfluorobutane sulfonate (PFBS) and trichloroethene (TCE) at boron-doped diamond film electrodes and the adsorption of PFOS and PFBS on granular activated carbon and ion exchange resins.

Experiments measuring oxidation rates of PFOS and PFBS were performed over a range in current densities and temperatures using a rotating disk electrode (RDE) reactor and a parallel plate flow-through reactor. Oxidation of PFOS was rapid and yielded sulfate, fluoride, carbon dioxide and trace levels of trifluoroacetic acid. Oxidation of PFBS was slower than that of PFOS. A comparison of the experimentally measured apparent activation energy with those calculated using Density Functional Theory (DFT) studies indicated that the most likely rate-limiting step for PFOS and PFBS oxidation was direct electron transfer. The costs for treating PFOS and PFBS solutions were compared and showed that PFOS is cheaper to degrade than PFBS.

Screening studies were performed to find a viable adsorbent or ion exchange resin for concentrating PFOS or PFBS. Granular activated carbon F400

(GAC-F400) and an ion exchange resin, Amberlite IRA-458, were the best methods for adsorbing PFOS. Ionic strength experiments showed that the solubility of the compounds affected the adsorption onto solid phases. Regeneration experiments were carried out to determine the best method of recovering these compounds from the adsorbents; however, the compounds could not be effectively removed from the adsorbents using standard techniques.

The electrochemical oxidation of trichloroethene (TCE) at boron-doped diamond film electrodes was studied to determine if this would be a viable degradation method for chlorinated solvents. Flow-through experiments were performed and showed TCE oxidation to be very rapid. Comparing the data from the DFT studies and the experimentally calculated apparent activation energies the mechanism for TCE oxidation was determined to be controlled by both direct electron transfer and oxidation via hydroxyl radicals.

CHAPTER 1

INTRODUCTION

1.1 Outline

This dissertation consists of five chapters. Chapter 1 describes the motivation behind the research performed. Chapter 2 explores the degradation of perfluorooctane sulfonate with boron-doped diamond film electrodes. Chapter 3 compares the degradation of perfluorobutane sulfonate with that of perfluorooctane sulfonate using electrochemical oxidation. Chapter 4 investigates the use of different adsorption methods to concentrate perfluorooctane sulfonate and perfluorobutane sulfonate from dilute aqueous systems. Chapter 5 focuses on the electrochemical oxidation of trichloroethylene using boron-doped diamond film electrodes.

1.2 Introduction

Perfluorinated and chlorinated organic compounds, such as perfluorooctane sulfonate and trichloroethylene, are found as contaminants in aqueous systems throughout the world. The most common method of removing TCE is air stripping followed by adsorption onto granular activated carbon. Reverse osmosis, advanced oxidation processes or incineration have been used to remove PFOS from contaminated waters. However, these technologies either concentrate these compounds or destroy them while producing hazardous by-products. Electrochemical oxidation presents a method of completely removing

these compounds from aqueous systems while leaving products that are inert to the environment. The introduction of boron-doped diamond film electrodes offers a stable electrode with the ability to degrade a wide range of contaminants, and allows electrochemical treatment to become an emerging technology in wastewater treatment (*1 - 4*).

Boron-doped diamond film electrodes are composed of a p-silicon substrate with a diamond layer that is deposited using Chemical Vapor Deposition (*5*). The diamond is doped with boron to make the electrodes more conductive. The advantages of these electrodes include: chemical inertness, low background current, high mechanical strength, and no catalyst that will leach or foul (*6 - 8*). These electrodes provide a wide potential window where neither reduction nor oxidation of water takes place at substantial rates (*9, 10*). These electrodes degrade different compounds using either direct electron transfer (*11*), hydroxyl radicals produced from water oxidation (*12 - 14*), or by producing oxidants from the background electrolyte, such as hypochlorite and persulfate (*15 - 17*). Various studies have shown that these electrodes can degrade a wide range of contaminants, including different organic compounds (*4, 7, 14 - 16, 18 - 28*), surfactants (*1, 2*), dyes (*29 - 31*), pesticides (*9, 32*) and nitrogenic compounds (*33*) from aqueous systems.

Figure 1-1 shows a proposed treatment scheme for the removal of PFOS and other organic compounds from aqueous systems. The objective of this research was to determine if perfluorooctane sulfonate (PFOS) and

trichloroethylene (TCE) can be oxidatively degraded by BDD electrodes. A comparison of the oxidation of perfluorobutane sulfonate (PFBS) and PFOS was also performed. This research also studied the different methods for concentrating PFOS and PFBS from dilute systems.

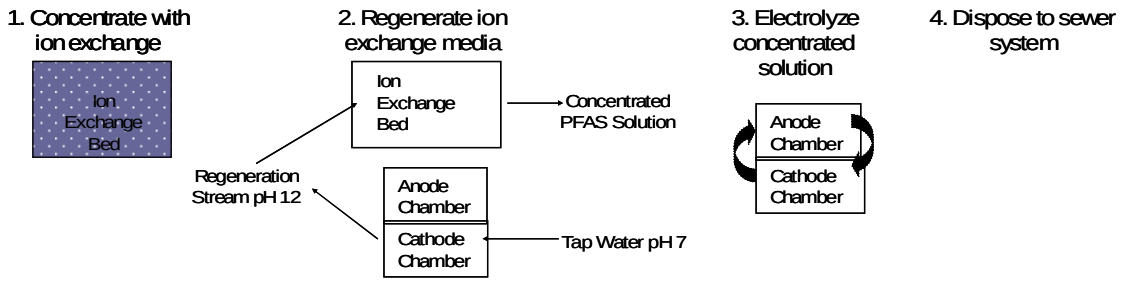

Figure 1-1: Proposed treatment scheme for PFOS and other organic compounds.

CHAPTER 2

OXIDATIVE DESTRUCTION OF PERFLUROOCTANE SULFONATE USING BORON DOPED DIAMOND FILM ELECTRODES

2.1 Abstract

This research investigated the oxidative destruction of perfluorooctane sulfonate at boron doped diamond film electrodes. Experiments measuring oxidation rates of PFOS were performed over a range in current densities and temperatures using a rotating disk electrode (RDE) reactor and a parallel plate flow-through reactor. Oxidation of PFOS yielded sulfate, fluoride, carbon dioxide and trace levels of trifluoroacetic acid. Reaction rates in the RDE reactor were zeroth order in PFOS concentration. Reaction rates in the flow-through reactor were mass transfer limited and were pseudo-first order in PFOS concentration, with a half-life of 5.3 minutes at a current density of 20 mA/cm^2. Eyring analysis of the zeroth order rate constants at a fixed electrode potential yielded an apparent activation energy of 4.2 kJ/mol for PFOS oxidation. Density functional theory (DFT) simulations were used to calculate activation barriers for different possible reaction mechanisms, including oxidation by hydroxyl radicals at different sites on the PFOS molecule, and direct electron transfer. A comparison of the experimentally measured apparent activation energy with those calculated using DFT indicated that the most likely rate-limiting step for PFOS oxidation was direct electron transfer.

2.2 Introduction

Perfluorooctane sulfonate (PFOS) ($C_8F_{17}SO_3^-$) is one of the most widely used perfluorinated organic compounds. PFOS is used in metal plating and semiconductor manufacturing, and is contained in a wide variety of household products, including: carpets, leather, paper, food containers, fabrics and fire-fighting foams (*34*). Because of the high stability of carbon-fluorine bonds (*35*), PFOS and other perfluorinated organic compounds are chemically stable and resistant to biodegradation. These properties have resulted in worldwide accumulation of perfluorinated compounds in the environment (*36 - 39*), in wildlife (*40 - 44*), and in humans (*45 -48*).

The accumulation of PFOS in the environment has promoted interest in destructive treatment methods for removing PFOS from aqueous solutions. Two studies have attempted to oxidize PFOS using advanced oxidation processes (AOPs) employing hydrogen peroxide with Fenton's reagent, ultraviolet light or ozone (*49, 50*); however, no PFOS oxidation observed in either study. Other less conventional methods have also been tested for their ability to degrade PFOS. Moriwaki *et al.* (*49*) used ultrasonication under both argon and oxygen atmospheres. Although they observed some PFOS degradation, reactions were slow, with PFOS half-lives ranging from 43 to 102 minutes. Additionally, the sonication process was not able to mineralize PFOS to CO_2, but instead yielded products, such as perfluorooctanoic and perfluouroheptanoic acids, that were more recalcitrant to oxidation. Hori *et al.* (*51*) used photooxidation with UV light

to oxidize PFOS. There was no oxidation unless the experiments were performed under a high-pressure (4.8 bar) oxygen atmosphere. PFOS oxidation was slow, with a half-life of 22 hours and the products were more recalcitrant, lower molecular weight perfluorinated organic acids. Hori *et al*. (*52*) also investigated the use of iron powder in 350 °C subcritical water for treating PFOS. After 6 hours a fluoride yield of approximately 50% was observed, but other products were not identified.

Electrochemical oxidation can overcome the limited oxidizing abilities of conventional AOPs, since potentials on the electrodes can be made much more oxidizing than hydroxyl radicals. In fact, oxidation of hydroxyl radicals is an important step in the oxygen evolution reactions that occur on anode surfaces under water treatment conditions (*53*). The recent advent of boron doped diamond (BDD) film electrodes has accelerated the development of electrochemical water treatment technologies (*54*).

This research investigated the effectiveness of BDD electrodes for oxidizing PFOS in dilute aqueous solutions. Reaction rates and reaction products were measured in both flow-through and rotating disk electrode reactors. The effects of current density and temperature on reaction rates were used to elucidate the rate-limiting step for PFOS oxidation. Quantum mechanical simulations using density functional theory (DFT) were used to evaluate potential energy barriers associated with different reaction mechanisms.

2.3 Materials and Methods

Rotating Disk Electrode Reactor Experiments measuring PFOS reaction rates were performed in a custom glass cell with a solution volume of 310 mL. The working electrode consisted of a 1.1 cm diameter disk composed of a BDD film on a p-silicon substrate (Adamant Technologies, Neutchatel, Switzerland). The disk electrode was operated using a rotating disk electrode (RDE) assembly (Princeton Applied Research, PAR, Oak Ridge, TN) rotated at 3000 revolutions per minute to eliminate mass transfer limitations. A 12 cm long by 0.3 mm diameter platinum wire (Aesar, Ward Hill, MA) served as the counter electrode and a Hg/Hg_2SO_4 electrode (PAR) saturated with K_2SO_4 served as the reference electrode. Currents and electrode potentials were controlled using a model 273A potentiostat (PAR). All potentials were corrected for uncompensated solution resistance and are reported with respect to the standard hydrogen electrode (SHE) by adding 0.64 V to the Hg/Hg_2SO_4 electrode potentials. Experiments were performed over temperatures ranging from 17 to 47 ^oC and were controlled using a recirculating water bath.

An initial PFOS concentration of ~0.4 mM was used in all experiments. The PFOS solutions were prepared from heptadecafluorooctanesulfonic acid solution (Fluka, St. Gallen, Switzerland) and had an initial pH value of 4. Experiments were performed in 7.5 and 10 mM $NaClO_4$ background electrolyte solutions, and in solutions without any background electrolyte. Samples were

taken periodically to determine PFOS removal and reaction products. Solution pH values were measured using a Symphony® pH electrode (VWR, Bristol, CT).

Flow Through Reactor In order to prevent the loss of volatile reaction products that occurred in the RDE reactor, experiments were also performed in a gas-tight, flow-through reactor. The working and counter electrodes consisted of BDD films on p-silicon and were obtained from Adamant Technologies. The flow through reactor contained one bipolar and two monopolar electrodes that were 5 cm long and 2.5 cm wide. The bipolar electrode was situated between the two monopolar electrodes with an interelectrode gap of 3 mm. The monopolar electrodes were connected to a Protek (Stayton, OR) model 3050 direct current power supply. The flow-through cell was operated galvanostatically and no reference electrode was used. The two anodes in the cell provided a total anodic surface area of 25 cm^2. The cell had a solution capacity of 15 mL, which yielded a surface area to volume ratio of 1.67 cm^{-1}.

The flow-through reactor was operated in a closed-loop system containing a 2.5 L liquid chromatography reservoir and a peristaltic pump connected via Teflon® tubing. Experiments were performed by recirculating 2 L of a solution containing 0.4 mM PFOS in 10 mM $NaClO_4$ background electrolyte at a rate of 100 mL/min. The reservoir was connected to a pressure gauge via a 0.635 cm (o.d.) stainless steel column containing a palladium catalyst (Aldrich). The catalyst was used to promote H_2 oxidation to water in order to prevent pressure build-up from the gases produced from water electrolysis. The solutions were

sampled over time to determine PFOS removal and products formed. To account for only the time that the fluid spent in the reactor, the elapsed electrolysis times were calculated from:

$$\text{electrolysis time} = \text{elapsed real time} \times \frac{\text{reactor volume}}{\text{total fluid volume in the system}} \qquad (2\text{-}1)$$

Product Analysis Samples were analyzed for PFOS and ionic reaction products using an ICS-3000 ion chromatograph (IC) with a conductivity detector (Dionex, Sunnyvale, CA) and an Acclaim Polar Advantage II C18 column (4.6 x 250 mm). Mixtures of 20 mM boric acid and 95% acetonitrile in water were used as the mobile phase. Program was run for 13.1 minutes and a gradient flow of the mobile phases varied from 25% to 45% acetonitrile and 75% to 55% boric acid. Fluoride and sulfate were analyzed using a Dionex DX 500 ion chromatograph with a conductivity detector and an Ion Pac AS18 column (4 x 250 mm) with an AG18 pre-column (4 x 50 mm). Headspace samples were analyzed for volatile products using gas chromatography/mass spectrometry (GC/MS) and aqueous samples were analyzed for nonvolatile products using liquid chromatography/mass spectrometry (LC/MS) by the University of Arizona Department of Chemistry Mass Spectrometry Facility.

Quantum Mechanics Simulations Density functional theory (DFT) simulations were performed to investigate possible PFOS reaction mechanisms. DFT calculations were performed using the DMol3 (*55*, *56*) package in the Accelrys Materials Studio (*57*) modeling suite using a personal computer operating with a 2.8 GHz Pentium 4 processor. All simulations used double-numeric with

polarization (DNP) basis sets (*58*) and the gradient corrected Vosko-Wilkes-Nair-Becke-Parr (VWN-BP) functionals for exchange and correlation (*59* -*61*). The nuclei and core electrons were described by DFT optimized semi-local pseudopotentials (*62*). Implicit solvation was incorporated using the COSMO (*63*) polarized continuum model.

Transition state searches were performed using a quadratic synchronous transit (QST) method (*64*) and refined using an eigenvector following method (*65*). The energy optimized structures and transition states were verified by frequency calculations. Imaginary frequencies with wave numbers smaller than 30 cm^{-1} were considered numerical artifacts of the integration grid and convergence criteria (*66*).

2.4 Results and Discussion

Figure 2-1 shows PFOS concentrations as a function of electrolysis time for current densities ranging from 1 to 20 mA/cm^2 at a temperature of 22°C. Reaction rates were zeroth order in PFOS concentration over the entire range of current densities. This behavior is indicative of reactive site saturation at the electrode surface. PFOS reaction rates in solutions without a supporting electrolyte were similar to those in 7.5 mM $NaClO_4$, as shown in Figure 2-2.

The correlation coefficient of r^2=0.196 between the rate constants and the current density indicates that reaction rates were only weakly dependent on the current density, as shown in Figure 2-2. Faradaic current efficiencies, defined as

the fraction of the cell current going towards PFOS oxidation, declined with increasing current density. The Faradaic current efficiency was calculated using the following equation:

$$\eta = \frac{k\,n}{F} \tag{2-2}$$

where k is the rate constant, n is the number of electrons per mole of contaminant degraded, and F is Faraday's constant, 9.6485 x 10^4 Coulombs/mole of electrons. Assuming complete oxidation requires 34 electrons per PFOS molecule (4 per carbon atom and 2 for sulfur), the Faradaic current efficiencies ranged from 100% at a current density of 1 mA/cm^2 to 20% at a current density of 20 mA/cm^2, as shown in Figure 2-3.

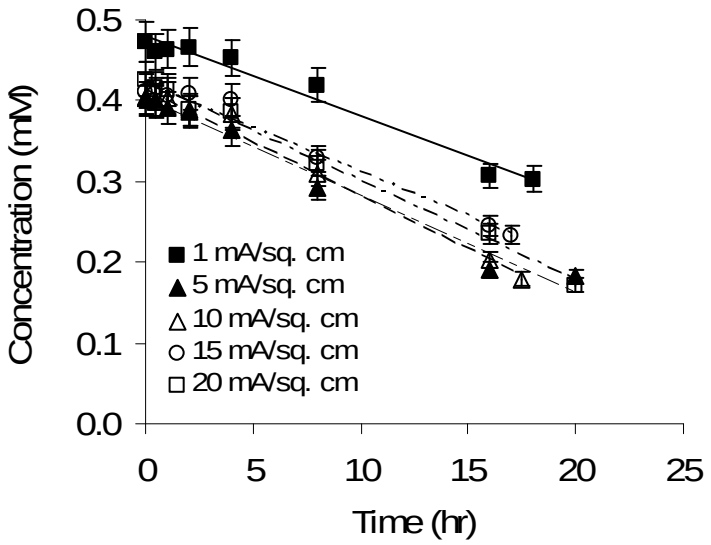

Figure 2-1: PFOS concentrations in the RDE reactor as a function of electrolysis time at current densities ranging from 1 to 20 mA/cm^2 at 22 °C in a 7.5 mM $NaClO_4$ electrolyte solution. The zeroth order rate constants at current densities of 1, 5, 10, 15 and 20 mA/cm^2 are: 0.0099, 0.0136, 0.0132, 0.0110, and 0.0123 mM/hr, respectively.

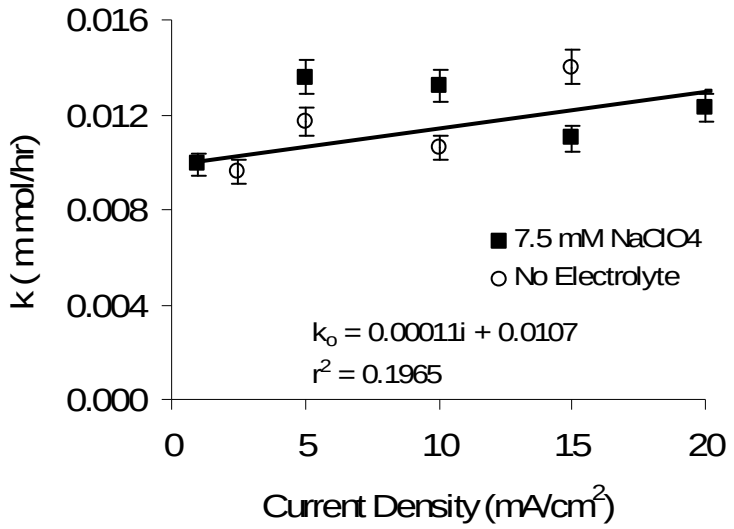

Figure 2-2: Zeroth order rate constants (k_o) as a function of the current density (*i*) for the data in Figure 1 measured in 7.5 mM $NaClO_4$ background electrolyte solutions. Also shown are zeroth order rate constants measured in solutions with out a background electrolyte.

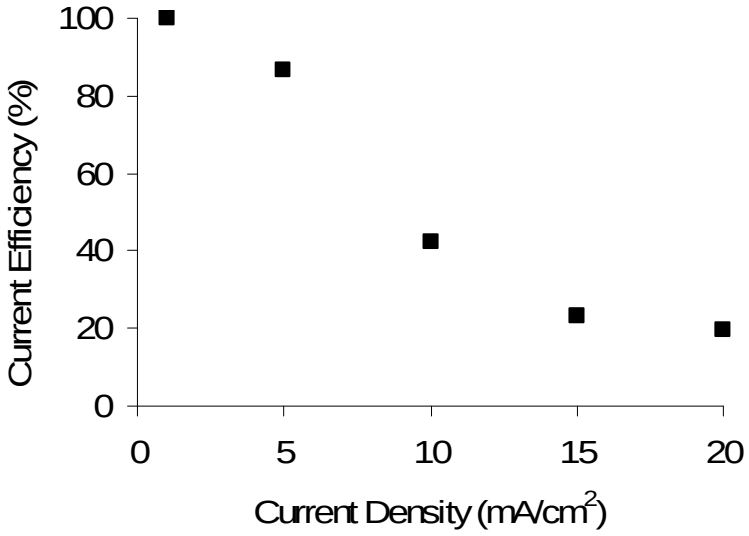

Figure 2-3: Faradaic current efficiency as a function of the current density for the data in Figure 2-1.

The detectable reaction products consisted of sulfate, fluoride, and trace levels of trifluoroacetic acid (TFA). Over the course of the experiments, the measured solution pH values decreased from 4 to ~2.3**,** which is indicative of carbonic acid production. The trace amounts of TFA recovered represented less than 3% of the PFOS removed. One sulfate and an average of 11±0.5 fluoride ions were produced per PFOS oxidized. The recovery of only 11 out of 17 fluoride ions per PFOS removed indicates that there were losses of volatile compounds from the solution. These volatile compounds likely include TFA, HOF and possibly HF. Loss of hypofluorite (HOF) from the solution was qualitatively indicated by the presence of a bleach-like odor.

To prevent the loss of volatile compounds, experiments were also performed in a gas-tight, flow-through reactor. Figure 2-4 shows the decline in PFOS and TOC concentrations as a function of the electrolysis time at a current density of 20 mA/cm^2 and 22 °C. Both the PFOS and TOC reaction rates in the flow-through reactor were first order in concentration. The difference in reaction order between the flow-through and RDE experiments can be attributed to mass transfer limitations in the flow-through reactor. For example, using the surface area to solution volume ratio in the flow-through reactor, the zeroth order rate constant measured using the RDE at a current density of 20 mA/cm^2 predicts complete PFOS removal in the flow-through reactor after only 8 minutes.

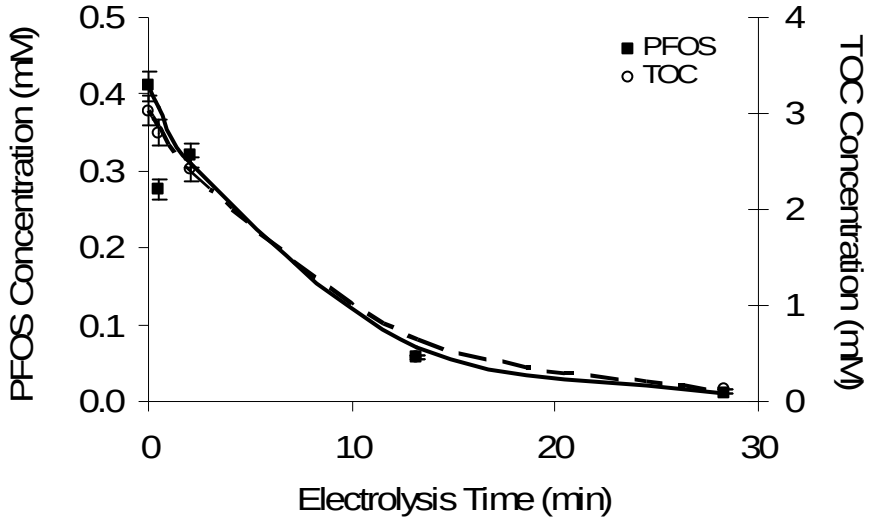

Figure 2-4. PFOS and TOC concentrations as a function of electrolysis time in the flow-through reactor operated at a current density of 20 mA/cm^2 at 22 °C with a 10 mM $NaClO_4$ electrolyte solution. Error bars represent the 95% confidence intervals of the analyses and the lines represent pseudo-first order model fits to the data. The pseudo- first order rate constants for PFOS and TOC removal are 0.13 and 0.12 min^{-1}, respectively.

The reaction products in the flow-through system were the same as those in the RDE reactor, except for a greater fluoride mass balance. The fluoride mass balance in the flow-through reactor increased to 14 out of 17. Only trace levels of TFA, representing less than 3% of the PFOS removed, were detected. The similar removal rates for PFOS and TOC confirm that intermediate organic reaction products in the solution were below quantifiable levels. This indicates that intermediate reaction products underwent complete oxidation before re-entering the bulk solution. The absence of solution phase organic reaction products for organic compound oxidation at BDD electrodes has been previously reported (*67, 68*).

Previous investigations have attributed organic compound oxidation at BDD electrodes to oxidation by hydroxyl radicals produced from water electrolysis (*67 - 71*). An alternative oxidation mechanism is the direct transfer of electrons from PFOS to the BDD anode. Evidence for these mechanisms can be obtained by measuring the activation energy for PFOS oxidation and comparing it to DFT calculated activation barriers for possible reaction mechanisms.

PFOS oxidation rates were measured at a constant electrode potential of 3.2 V/SHE at temperatures ranging from 17 to 47 °C. A potential of 3.2 V/SHE was used because it produced current densities similar to those used in Figure 2-1 (*i.e.*, ~1-10 mA/cm^2). Reaction kinetics that were zeroth order in PFOS concentration were observed at all four temperatures. Arrhenius equation:

$$k = A \exp\left(-\frac{E_a}{RT}\right) \tag{2-3}$$

where k is the rate constant, E_a is the activation energy (J/mol), R is the universal gas constant, 8.314 J/mol K, and T is the temperature (K) was used, with an Eyring plot of the zeroth order rate constants, to calculate the activation energy for the degradation of PFOS. The apparent activation barrier of 4.2 kJ/mol was calculated as shown in Figure 2-5. Activation barriers this small are normally indicative of unactivated processes, and are often attributable to temperature effects on diffusion rates (*72*).

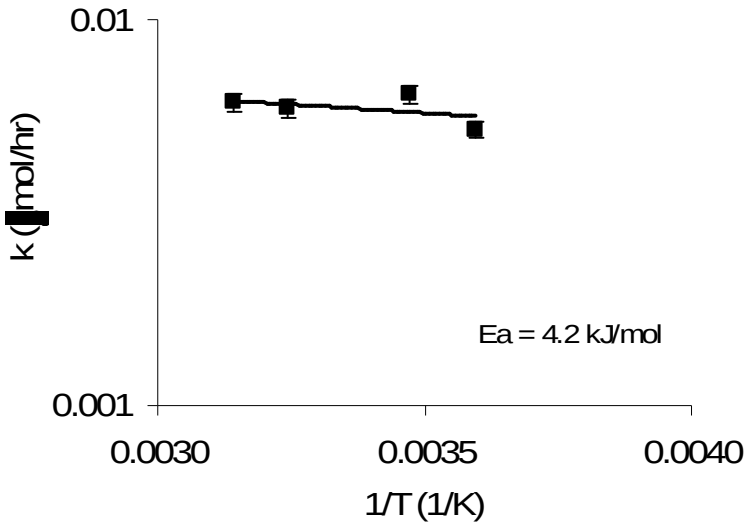

Figure 2-5: Eyring plot of the zeroth order rate constants measured at a fixed electrode potential of 3.2 V/SHE in the RDE reactor using a 7.5 mM $NaClO_4$ electrolyte solution. Error bars represent the 95% confidence interval of the analyses.

The experimental activation barrier can be compared to those for oxidation by hydroxyl radicals and for direct electron transfer. DFT simulations were used to investigate the activation barriers for reaction of hydroxyl radicals at three different sites on the PFOS molecule. Configurations of the initial reactants and final products are shown in Figures 2-6 to 2-8.

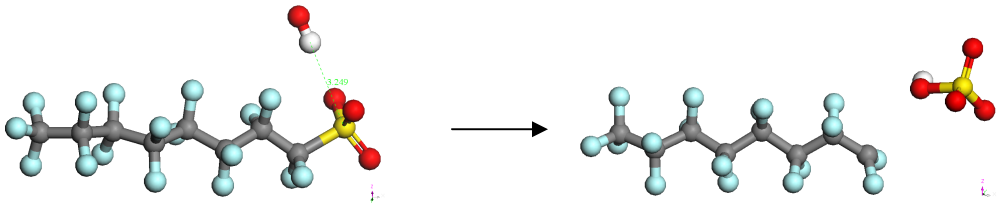

Figure 2-6: Initial reactants and final products for hydroxyl radical attack at the $-SO_3$ site. Atom key: C-gray, F-blue, S-yellow, H-white and O-red.

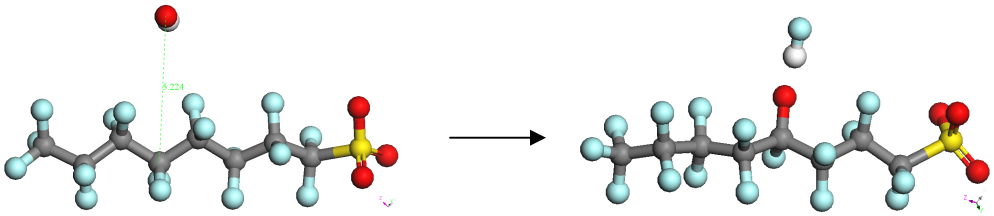

Figure 2-7: Initial reactants and final products for hydroxyl radical attack at the –F site. Atom key: C-gray, F-blue, S-yellow, H-white and O-red.

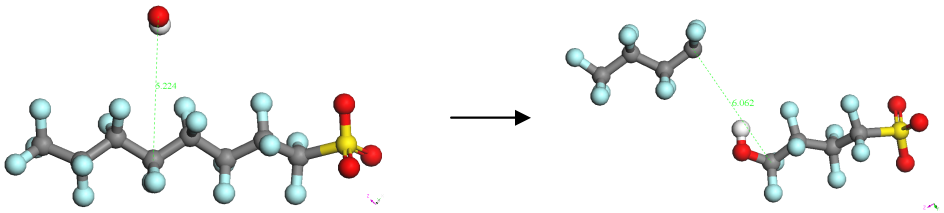

Figure 2-8: Initial reactants and final products for hydroxyl radical attack at a carbon-carbon bond. Atom key: C-gray, F-blue, S-yellow, H-white and O-red.

Figure 2-9a shows the transition state for reaction of $HO^{\bullet}$ with the $-SO_3$ group. This reaction produces HSO_4^- and a perfluorooctyl radical. The overall reaction energy is -116 kJ/mol, and the activation barrier determined from the transition state is 122 kJ/mol. Figure 2-9b shows the transition state for attack of $HO^{\bullet}$ at a fluorine atom. The oxygen of the hydroxyl radical replaces a fluorine atom on PFOS and HF is produced. The overall reaction energy is -89 kJ/mol and the activation barrier is 241 kJ/mol. Figure 2-9c shows the transition state for $HO^{\bullet}$ attack at a carbon-carbon bond in PFOS. The reaction produces a perfluorobutyl radical and 1-hydroxyperfluorobutane sulfonate, with an overall reaction energy of -152 kJ/mol and an activation barrier of 169 kJ/mol.

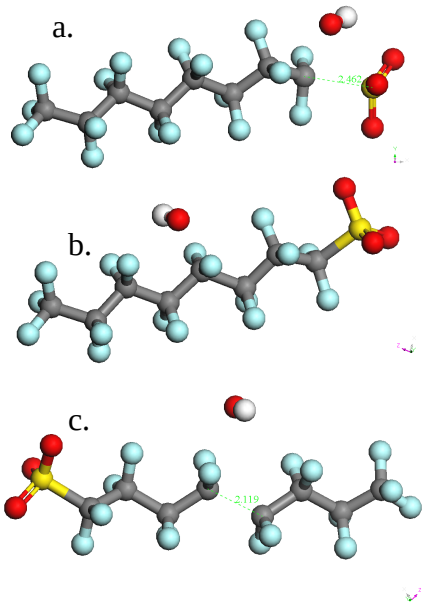

Figure 2-9. Transition state for hydroxyl radical attack at: a) the $–SO_3$ site, b) an –F site, and c) a C-C bond. Atom key: C-gray, F-blue, S-yellow, H-white and O-red.

The activation barriers calculated for reaction of hydroxyl radicals with PFOS are much greater than the measured activation energy of 4.2 kJ/mol. Additionally, the calculated barriers are much greater than those observed for hydroxyl radical oxidation of highly recalcitrant perchlorinated biphenyls, which are reported to range from 71 to 93 kJ/mol (*73*, *74*). However, the high calculated activation barriers are consistent with the lack of reaction observed for PFOS with conventional peroxide based AOPs (*49*, *50*), and indicate that the rate-limiting step for PFOS oxidation does not involve oxidation by hydroxyl radicals.

Activation energies for direct oxidation of PFOS have been calculated as a function of the electrode potential using the methods described in Anderson and Kang (*75*). DFT simulations indicate that loss of one electron leads to

lengthening of the C-S bond, and that the C-S bond length closely approximates the reaction coordinate (*i.e.*, >90% of the energy change between the reactant and the transition state is due to C-S bond lengthening). Figure 10a shows the energy of the reactant and products for the reaction:

$$C_8F_{17}SO_3^- \rightarrow C_8F_{17}SO_3^{\bullet} + e^- \qquad (2\text{-}4)$$

as a function of the C-S bond length at a potential of 2.5 V/SHE. The reactant energies were calculated by varying the length of the C-S bond from its minimum energy length of 1.91 Å, followed by geometry optimization of the structure. The product energies were calculated using the atomic positions determined from the optimized reactant structures, followed by self consistent field optimization of the electronic configurations. Having the products and reactants with identical atomic positions is justified by the Born-Oppenheimer approximation that changes in electronic configuration happen much faster than changes in atomic configuration (*76*). Energies from the vacuum scale were converted to the SHE scale by subtracting 4.6 eV (*75*). Product energies as a function of electrode potential were determined by shifting the energy profile of the product species downwards by 96.5 kJ (*i.e.*, 1.0 eV) to increase the electrode potential by 1.0 V and upwards by 96.5 kJ to decrease the electrode potential by 1.0 V (*75*). Intersection of the product and reactant energy profiles yields the bond length of transition state and the activation energy for the reaction, as illustrated in Figure 2-10a. The higher the electrode potential, the shorter the C-S bond stretching required for the reactant and product energy profiles to intersect. By shifting the

products energy profile up and down, activation energies as a function of electrode potential were calculated, as shown in Figure 2-10b.

Figure 2-10b shows that the activation barrier for PFOS oxidation decreases from 184 kJ/mol at an electrode potential of 1.6 V/SHE to 0 kJ/mol at a potential of 2.7 V/SHE. The experiments performed in this investigation were performed at electrode potentials ranging from 2.5 to 4.2 V/SHE. Therefore, the experiments were performed at sufficiently high overpotentials that the reactions could proceed without little or no activation barrier (*77*). In other words, there were electronic energy levels in the BDD electrode that were lower than the energy level of the highest occupied molecular orbital in an unactivated PFOS molecule.

The agreement of the DFT calculated activationless barrier for direct electron transfer at potentials >2.7V/SHE and the very low experimentally measured activation energy at 3.2 V/SHE indicates that direct electron transfer is the most likely rate-limiting mechanism for PFOS oxidation.

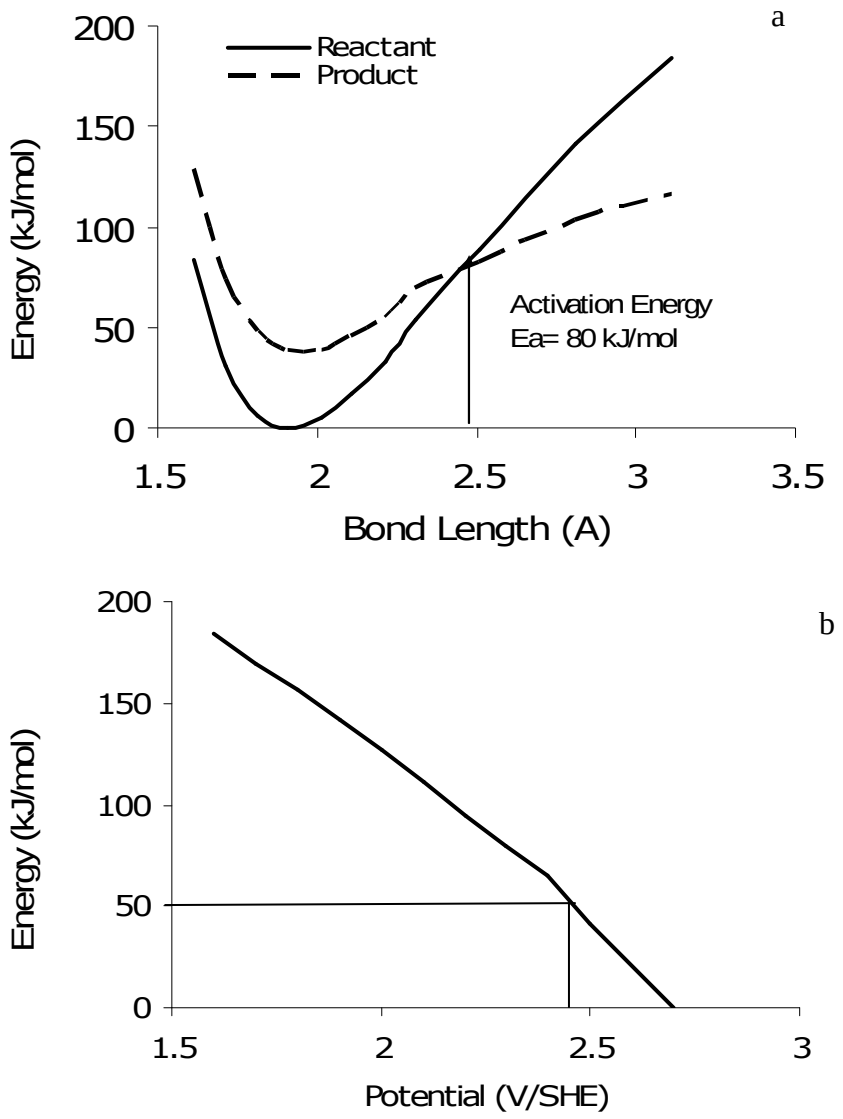

Figure 2-10. a) Energy profiles as a function of the C-S bond length at an electrode potential of 2.5 V/SHE for the reactant ($C_8F_{17}SO_3^-$) and products ($C_8F_{17}SO_3^{\bullet} + e^-$) for vertical electron transfer. b) Activation energies as a function of electrode potential for direct oxidation based on the calculations in part (a).

2.5 Acknowledgements

Thanks to the National Science Foundation Chemical and Transport Systems Directorate (CTS-0522790), the Semiconductor Research

Corporation/Sematech Engineering Research Center for Environmentally Benign Semiconductor Manufacturing (2001MC425), and the Donors of the American Chemical Society Petroleum Research Fund (PRF 43535-AC5) for support of this work.

CHAPTER 3

COMPARISON OF THE OXIDATIVE DESTRUCTION OF PERFLUOROBUTANE SULFONATE TO THAT OF PERFLUOROOCTANE SULFONATE USING BORON-DOPED DIAMOND FILM ELECTRODES

3.1 Abstract

Chapter 3 compares the electrochemical degradation of PFOS and PFBS at boron-doped diamond film electrodes using rotating disk electrode (RDE) and flow-through reactors. Density functional theory (DFT) calculations were also performed to determine the rate-limiting mechanism for PFBS oxidation. The DFT calculations showed that the rate-limiting mechanism for PFBS oxidation involved direct electron transfer and was the same as that for PFOS. In the RDE reactor, zeroth order rate constants for PFBS oxidation ranged from 3 to 11 times smaller than those for PFOS. In the flow-through reactor, first-order rate constants for PFBS were oxidation were 1.5 times smaller than those for PFOS at the same current density. The slower reaction rates for PFBS versus PFOS can likely be attributed to a factor of 2.2 greater apparent activation energy for PFBS. The costs for treating PFOS and PFBS solutions were compared and showed that PFOS is cheaper to degrade than PFBS using both 10 mA/cm^2 and 20 mA/cm^2.

3.2 Introduction

Perfluorooctane sulfonate (PFOS) is the most commonly used and detected PFAS compound in the semiconductor industry and around the world. Studies have revealed that PFOS accumulates in the tissues and organs of

humans, fish and other animals (*78* - 80) and has been determined in waters around the world (*81* - *84*). The accumulation of PFOS in the environment has led to the banning of perfluorinated compounds from the Unites States by the Environmental Protection Agency (EPA). The ban on these compounds has led the semiconductor industry to replace PFOS with perfluorobutane sulfonate (PFBS). Like PFOS, PFBS accumulates in the environment and is non-biodegradable.

Various destruction methods are being studied for the degradation of different perfluoroalkyl sulfonate (PFAS) compounds including sonochemical degradation, advanced oxidation processes, and ultraviolet irradiation (*85* - *88*). Since the semiconductor industry has started replacing PFOS with PFBS in its fabrication processes, a comparative assessment of the electrochemical degradation of these compounds will be useful to determine the possible environmental implications of replacing PFOS with PFBS. This chapter compares the electrochemical degradation of PFBS and PFOS at boron-doped diamond film electrodes and will compare the cost of treatment for the two compounds.

3.3 Materials and Methods

Rotating Disc Electrode (RDE) Reactor Experiments using a rotating disc electrode were performed to determine the rates of reaction for the destruction of PFBS. The experiments performed were similar to those for PFOS as discussed in Chapter 2.

Flow through Reactor Experiments were performed in the same MiniDiacell® (Adamant Technologies) flow-through reactor containing two monopolar and one bipolar BDD on p-silicon electrodes. The total anode surface area of 25 cm^2 and the void volume of 15 mL yielded a surface area to solution volume ratio of 1.67 cm^2 mL^{-1}. Experiments were performed by placing 1 L of 0.4 mM PFBS in 10 mM $NaClO_4$ into the reservoir. During the electrolysis experiments the solution was pumped through the reactor at a flow rate of 10.0 mL min^{-1} and periodically sampled for PFBS and product concentrations. The electrolysis times were calculated according to equation 2-1, which accounts for the time that each molecule in the reactor was subject to electrolysis.

Product Analyses PFBS concentrations were determined a Dionex (Sunnyvale, CA) ICS-3000 ion chromatograph (IC) equipped with an autosampler, an Acclaim Polar Advantage II C18 column (4.6 × 250 mm), and an electrical conductivity detector. The mobile phase was the same as that of the PFOS concentration analysis in Chapter 2. Samples were analyzed for fluoride and sulfate, the method can be found in chapter 2.

3.4 Results and Discussion

Table 3-1 shows the properties of different forms of PFOS and PFBS. Looking at the properties, PFBS is approximately one and one half times smaller and four times more soluble than PFOS in pure water. Also note that the

potassium salt of PFOS has a higher solubility than the acid form of the compound.

Compound	H-PFBS	H-PFOS	K-PFOS
Molecular Formula	$C_4F_9SO_3H$	$C_8F_{17}SO_3H$	$C_8F_{17}SO_3K$
Molecular weight (g/mol)	338.13	500.13	538.13
Density (g/cm^3)	1.87	1.25	N/A
Boiling Point (^oC)	210-212	258-260	N/A
Solubility (mg/L)	2300	350-570	498-680

Table 3-1: Properties of PFBS and PFOS (where H – Acid form and K- Potassium salt).

Figure 3-1a shows PFBS concentrations as a function of electrolysis time at a current density of 10 mA/cm^2. The oxidation of PFBS in the flow-through reactor follows first order kinetics. Figure 3-1b shows the fraction of PFBS and PFOS removed from the aqueous system in the flow-through reactor. The current density for the PFOS was at both 20 mA/cm^2 and 10 mA/cm^2. The current density for the PFBS was the same as that in figure 3-1a. Figure 3-1b shows that the current density only made a slight difference in the amount of PFOS degraded. Comparing the PFBS degradation to that of PFOS, the half life of PFBS was ~10 minutes while the half life of PFOS was ~7.5 minutes at 10 mA/cm^2 and ~5 minutes at 20 mA/cm^2. So PFOS degradation is faster than PFBS degradation at the BDD electrode.

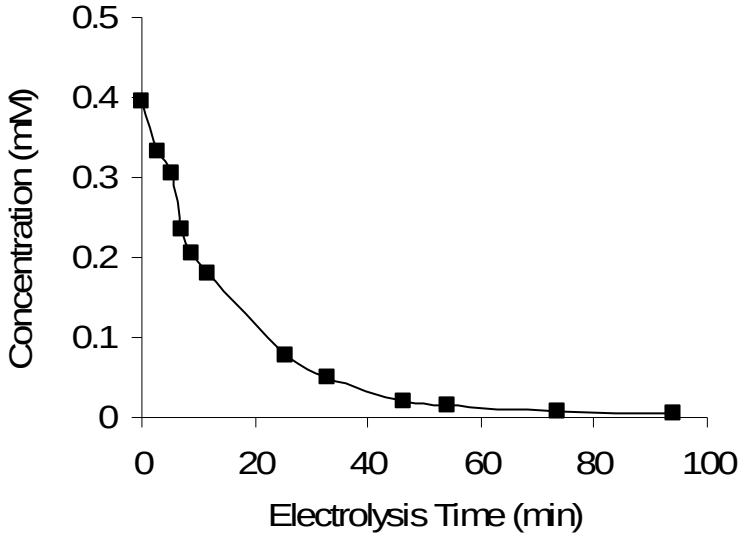

Figure 3-1a. Concentration of PFBS as a function of electrolysis time at current a density of 10 mA cm^{-2} in the flow-through reactor.

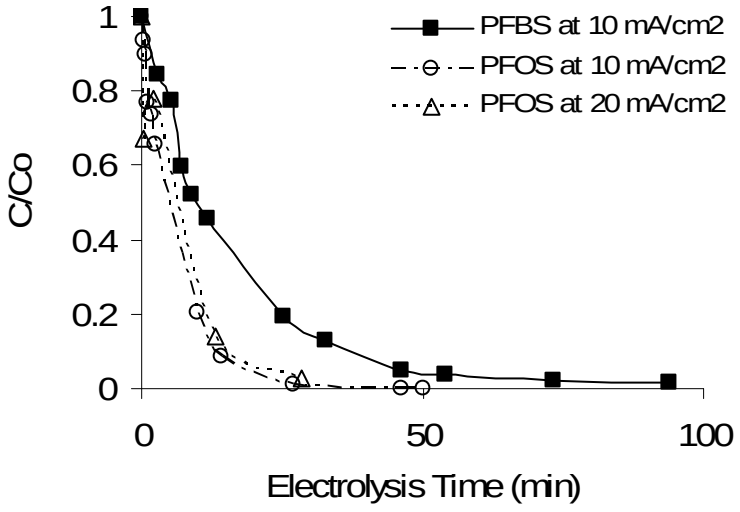

Figure 3-1b. Comparison of PFBS degradation with PFOS degradation in the flow-through reactor. PFBS degradation took place at a current density of 10 mA/cm2 while PFOS degradation took place at 20 mA/cm2 and 10 mA/cm2.

Figure 3-1c shows the sulfate and fluoride concentrations for the experiment described in Figure 3-1a. The oxidation products consisted of carbon dioxide, sulfate, fluoride, and trace amounts of trifluoroacetic acid (TFA). Trace levels of TFA represented <3% of the PFBS removed which was the same percentage of TFA that was present during the oxidation of PFOS. Over the course of the experiments, solution pH values decreased from 5 to 3 and the fluoride recovery was 8.2 ± 0.3 out of 9 fluoride ions per PFBS degraded. The average recovery of only 91% for fluoride may result from the loss of fluorinated species, such as HF and TFA, into the gas phase as was the case of PFOS oxidation.

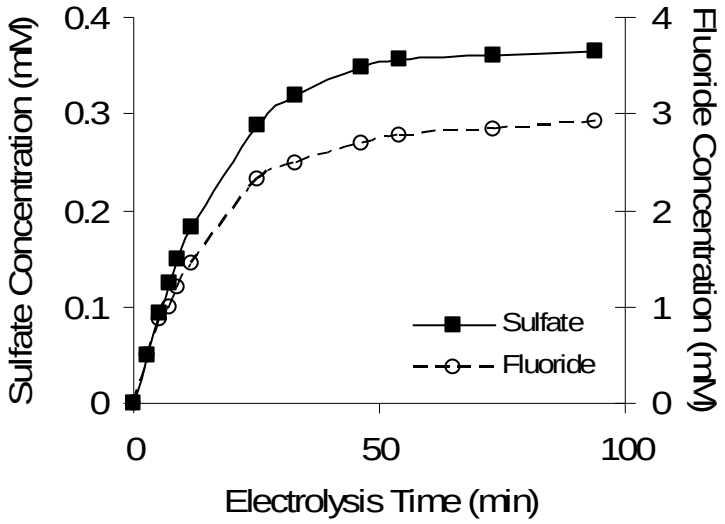

Figure 3-1c: Fluoride and sulfate concentrations as a function of electrolysis time for PFBS. Current density was 10 mA/cm2 in the flow through reactor.

Figure 3-2a shows PFBS concentrations in the RDE reactor at fixed current densities of 5, 10, 15, and 20 mA cm^{-2} at 22 °C. In all experiments, the

oxidation rate of PFBS was zeroth order in PFBS concentration and increased with increasing current density. This type of behavior was seen in Figure 2-1 for the PFOS experiments and is typical for surface reactions whose rates are limited by the availability of reaction sites over the entire concentration range investigated.

Figure 3-2b shows the zeroth order reaction rate constants for PFBS and PFOS at the RDE electrode. For PFBS the zeroth order reaction rate constants are 0.42, 0.91, 1.26, and 1.365 μM/hr for 5, 10, 15, and 20 mA/cm^2 respectively. These rates range from 3 to 11.5 times less than the rates for PFOS degradation at a BDD electrode at the same current density. Figure 3-3 shows the current efficiency for the degradation of PFBS. The current efficiency was determined using equation 2-2 and ranged from 3.3% for 20 mA/cm^2 to 4.4% at 10 mA/cm^2. The current efficiency suggests that the degradation of PFBS is optimized at 10 mA/cm^2.

To help determine the rate-limiting step temperature dependence studies were performed on the PFBS. The reaction rates for oxidation of PFBS were measured at 7, 15, 22, 25 and 45 °C. An Eyring plot was used to determine the apparent activation energies for PFBS oxidation and is illustrated in Figure 3-4. The data in Figure 3-4 yields an apparent activation energy of 9.3 ± 3 kJ mol^{-1}. Reactions with activation barriers this low generally proceed readily at room temperature (*89*). The activation barrier of PFBS is twice that of PFOS

suggesting that PFOS degradation would take place before PFBS degradation at room temperature.

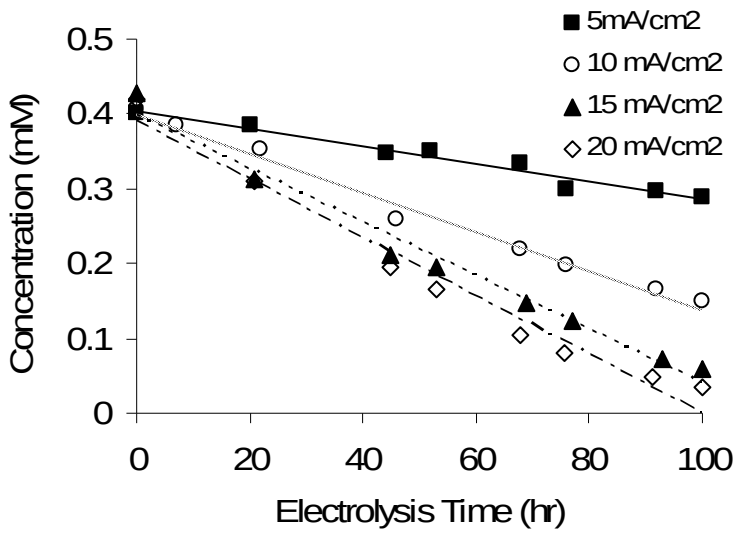

Figure 3-2a. PFBS concentration as a function of electrolysis time at current densities of 5, 10, 15 and 20 mA cm^{-2} in the RDE reactor.

DFT simulations were performed to determine the activation barriers for the reaction of hydroxyl radicals at different sites on the PFBS molecule. For hydroxyl radical attack at the $-SO_3^-$ group, the activation energy determined from the transition state was 123 kJ/mol. The activation energy for PFOS was 122 kJ/mol for the same reaction. As mentioned in chapter 2 this suggests that neither the PFOS nor PFBS would readily degrade at room temperature when undergoing hydroxyl radical attack.

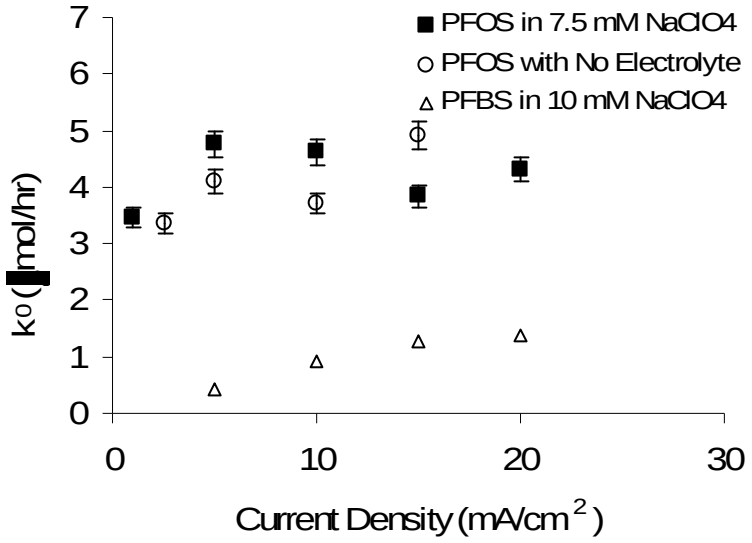

Figure 3-2b: Zeroth order rate constants for PFOS and PFBS as a function of the current density. Rate constants for PFOS are 3 to 11.5 times faster than those for PFBS.

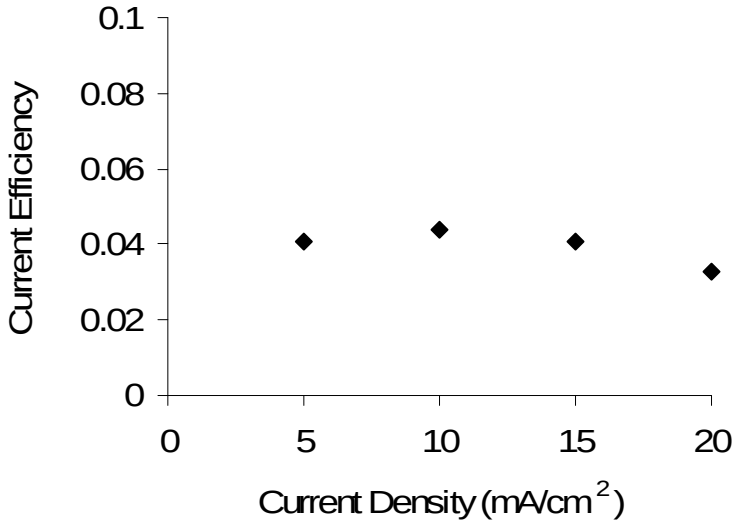

Figure 3-3: Current efficiency for the oxidation of PFBS in an RDE reactor at current densities of 5, 10, 15, and 20 mA/cm^2.

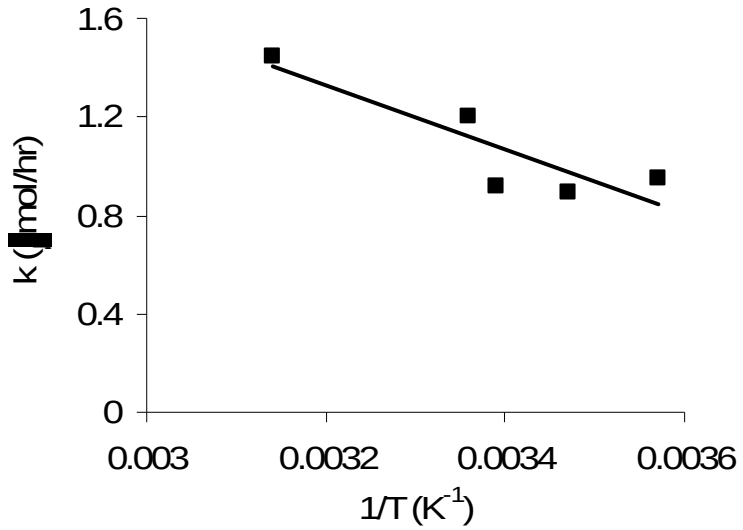

Figure 3-4: Erying plot of zeroth order rate constants for PFBS oxidation at a fixed current density of 10 mA cm^{-2}.

As with the PFOS, DFT simulations were used to determine the activation energies for direct oxidation of PFBS as a function of the electrode potential using the methods described in Chapter 2. Figure 3-5a shows the energy of the reactant (PFBS anion) and products (PFBS neutral radical + electron) as a function of the C-S bond length at a potential of 2.5 V/SHE. Intersection of the two energy profiles yields the bond length at the transition state and the activation energy for the reaction:

$$C_4F_9SO_3^- + e^- \rightarrow C_4F_9SO_3^* \qquad (3\text{-}1)$$

By shifting the products energy profile up and down, activation energies as a function of electrode potential were calculated, as shown in Figure 3-5b. Figure 3-5b shows that the activation energy decreases from 270 kJ mol^{-1} at a potential of 1.0 V/SHE to zero at a potential of 3.0 V/SHE. This indicates that the

reaction becomes activationless at potentials greater than 3.0 V/SHE, and is consistent with the low apparent activation energy calculated in Figure 3-4. For PFOS the reaction becomes activationless at potential greater 2.5 V/SHE. This suggests that more energy is needed to degrade PFBS than PFOS.

The faster reaction rates of PFOS versus PFBS can most likely be attributed to its lower apparent activation energy. The relative rates (r_1 and r_2) for two reactions with activation energies of E_{a1} and E_{a2} are given by:

$$\frac{r_1}{r_2} = \frac{A_1 \exp\left[-E_{a1}/RT\right]}{A_2 \exp\left[-E_{a2}/RT\right]} \qquad (3\text{-}2)$$

where A_1 and A_2 are the pre-exponential factors in Arrhenius rate expressions, R is the gas constant and T is temperature. Given the similar rate-limiting mechanisms, the pre-exponential factors A_1 and A_2 should be similar for both PFBS and PFOS oxidation. Therefore, given an E_{a1} of 4.2 kJ/mol for PFOS and an E_{a2} of 9.3 kJ/mol for PFBS, equation 3-2 predicts a factor of 8 faster reaction rate for PFOS than for PFBS. This is close to the value of 5.01 shown in figure 3-2b at a current density of 10 mA/cm^2, which is close to the current density at which the activation energies were measured. The fact that the rate differences were only a factor of two in the flow-through reactor can be attributed to mass transfer limitations on the observed reaction rates for both PFOS and PFBS.

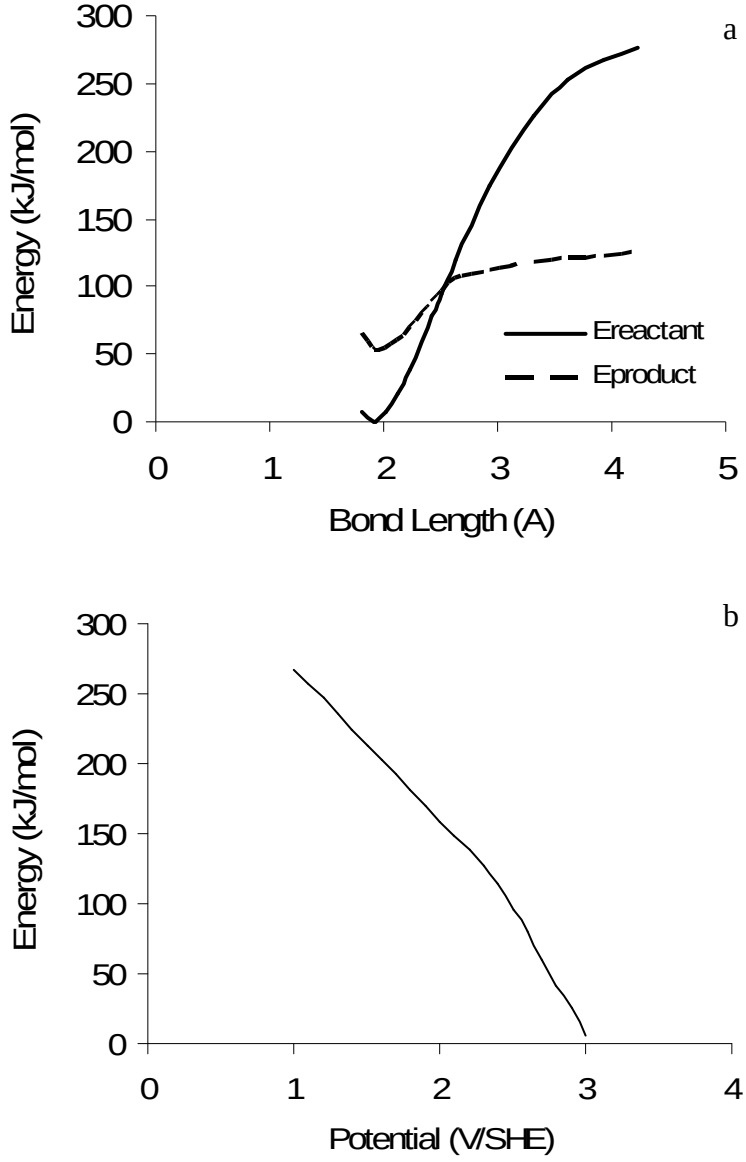

Figure 3-5: a) Energy profiles for reactant ($C_4F_9SO_3^-$) and products ($C_4F_9SO_3^\bullet + e^-$) for vertical electron transfer as a function of the C-S bond length at an electrode potential of 2.5 V/SHE. b) Activation energies as a function of electrode potential for a direct electron transfer reaction.

Energy and Cost Comparison The economic feasibility of using electrochemical oxidation to destroy PFOS and PFBS was compared by determining the electrical

costs of running a flow-through reactor. To determine the amount of current used a scaling factor was determined:

$$S_f = \frac{1000\text{gal} \times 3.785\ {}^{\text{L}}\!/\!_{\text{gal}}}{v} \qquad (3\text{-}3)$$

where S_f is the scaling factor and v is the volume of solution in the reactor at one time (L). Applying the scaling factor to the current gives:

$$I = i \times a_s \times S_f \qquad (3\text{-}4)$$

where I is the current needed to treat 1000 gal/L (A), i is the current density applied (A/cm^2) and S_f is the scaling factor.

The amount of time needed to degrade these compounds using the reaction rate constants from the flow-through reactors since this would simulate real life treatment of the wastewater. The following equation was used to determine the time:

$$t = -\frac{1}{k_1} \ln \frac{C}{C_0} \qquad (3\text{-}5)$$

where t is the time (hr), k_1 is the first order rate constant for the different flow-through experiments (hr^{-1}), C_0 is the influent concentration and C is the final concentration of 1 mg/L. The energy (kW hr) required to treat 1000 gal can be determined using the following equation:

$$\text{Energy} = \frac{I \times V \times t}{1000} \qquad (3\text{-}6)$$

where I is the current (A), V is the applied voltage (V), and t is the time (hr). The cost to treat 1000 gal of influent was determined by assuming the following equation:

$$\text{Dollars} = \$0.10/\text{kW hr} \times \text{Energy} \qquad (3\text{-}7)$$

Figure 3-6 shows the amount of energy needed to degrade PFBS using 10 mA/cm^2 current density and PFOS using 15 and 20 mA/cm^2 current density. Degradation of PFBS from 500 mg/L to 1 mg/L would require more energy than to degrade the PFOS from the same concentrations. This could be due to the fact that PFBS degrades at a slower rate than PFOS in the flow through reactor and would require more time and energy. Overall the cost of degrading both compounds from 500 mg/L to 1 mg/L would cost between $85.00 to $140.00 per 1000 gallons of wastewater. This is less expensive than other treatment processes capable of destroying perfluorinated compounds, such as combustion.

This study showed that PFBS can be readily oxidized at BDD electrodes while producing only trace amounts of organic products in the solution. The reaction rates to decompose PFBS were slow compared to those of PFOS. The cost of degrading PFBS or PFBS was less than $10/1000 gallon of water treated.

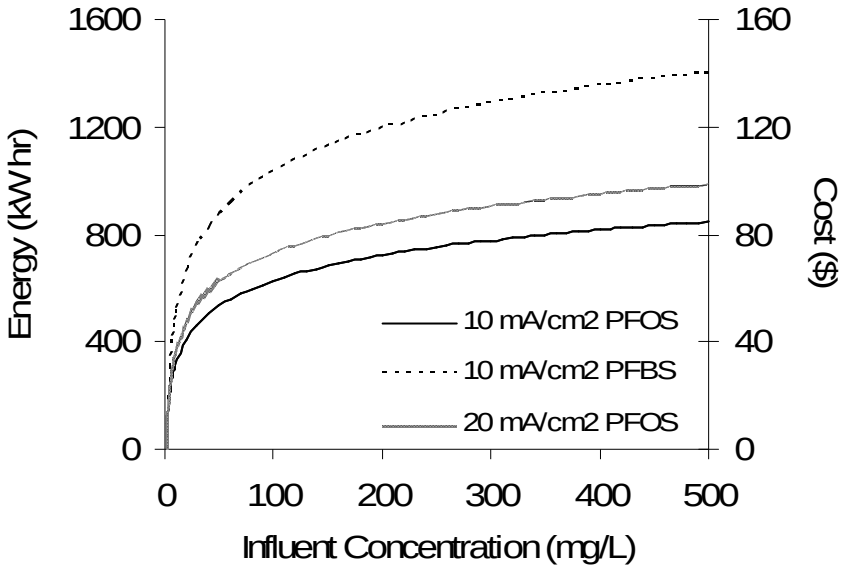

Figure 3-6: Cost and energy to degrade PFOS or PFBS to 1 mg/L from different influent concentrations. PFOS degradation was at 10 and 20 mA/cm^2 and PFBS was at 10 mA/cm^2.

3.6 Acknowledgements

Thanks to Zhaohui Liao for obtaining some of the data used in this chapter. Thanks to the National Science Foundation Chemical and Transport Systems Directorate (CTS-0522790) and to the Semiconductor Research Corporation /Sematech Engineering Research Center for Environmentally Benign Semiconductor Manufacturing (2001MC425), and the Donors of the American Chemical Society Petroleum Research Fund (PRF 43535-AC5) for support of this work.

CHAPTER 4

ADSORPTION OF PERFLUORINATED SURFACTANTS ON GRANULAR ACTIVATED CARBON AND ION EXCHANGE RESINS

4.1 Abstract

Chapter 4 looks at different methods of adsorbing PFOS and PFBS from dilute aqueous systems. Screening studies were performed on seven different adsorbents and one ion exchange resin to determine their ability for adsorbing PFAS compounds. These studies showed that granular activated carbon (GAC) and an ion exchange resin, Amberlite IRA-458, were the best methods for adsorbing PFOS. Kinetic and isotherm experiments were then performed on GAC and the IRA-458 and showed that the time required for equilibrium was approximately 50 hours for the GAC and 10 hours for the IRA-458. Heats of adsorption were used to investigate the adsorption mechanism and determine the conditions required for thermal regeneration. The heats of adsorption were endothermic and thus thermal regeneration via heating was not practical. Studies investigating the solubility of PFOS as a function of temperature and solution composition showed that the ionic strength of the solution and the type of counter ion affected the solubility of PFOS more than the temperature. Regeneration experiments were carried out to determine the best method of recovering these compounds from the adsorbents. Studies showed that while PFOS and PFBS adsorbed well to ion exchange resins and activated carbon, the compounds cannot be effectively removed from the adsorbents using standard techniques.

4.2 Introduction

In recent years perfluoroalkyl sulfonates have become a focal point for research due to their prevalence in the environment and their potentially adverse health effects on humans and animals. Perfluorooctane sulfonate (PFOS), which is the most widely used perfluorinated compound, has been reported in water, biota samples, human blood and liver samples, and wildlife worldwide (*90 - 93*).

Perfluoroalkyl sulfonates are organic molecules consisting of carbon chains where fluorine atoms have replaced hydrogen atoms. The strength of the carbon – fluorine bond makes these compounds highly stable and difficult to degrade. Advanced oxidation processes which add reagents such as ozone (O_3), O_3/UV, O_3/H_2O_2, and H_2O_2/Fe^{2+} (Fenton's reagent) have demonstrated to be ineffective in destroying PFOS and perfluorooctanoic acid (PFOA) (*94*).

These compounds are found in numerous industrial and consumer chemical products including surface treatment agents, paper protectors, refrigerants, pharmaceuticals, lubricants, adhesives, cosmetics, Teflon coatings, fire fighting foams and insecticides (*95*). The aviation and semiconductor industries use these surfactants as degreasing agents and in electroplating, electronic etching baths and as a photographic emulsifier (*96*).

Currently there are several disposal methods that have proven to be effective but carry with them several disadvantages. Among them are the release of these compounds into the environment, or combustion, which requires high temperatures and has been shown to produce haloacetic acid (*97*). Photochemical decomposition (*98, 99*),

sonochemical decomposition (*100*), zerovalent iron (*101*), reductive dehalogenation (*102*) and electrochemical oxidation at BDD anodes (*103*) have been shown to be effective for decomposing PFOS and other perfluorinated surfactants from aqueous solutions. Other studies have shown that reverse osmosis (*104*), granular activated carbon (GAC) (*105*) and ion exchange resins (*106*) can be used to remove PFOS from aqueous solutions.

Due to their occurrence in the environment, the U.S. Environmental Protection Agency (EPA) banned PFOS from the U.S. market in 2000 (*105*). However, due to the need for these compounds in several industries, in 2002 the U.S. EPA proposed a significant new use rule (SNUR) for perfluorooctanesulfonic acid and its salts which gave the semiconductor industry a waiver allowing them continued use of perfluorinated organic solvents. This waiver came with a stipulation that the industry had to find an alternative to PFOS, such as perfluorobutane sulfonate (PFBS), or a practical a way of disposing of or destroying these compounds.

While industries use PFOS in concentrated form, aqueous waste streams most often contain PFOS at low mg/L concentrations. This makes previously mentioned destructive method expensive to utilize. It is necessary to concentrate the PFOS in order to reduce the amount of wastewater being treated. The objective of this research is to compare different methods of concentrating PFOS and PFBS from dilute aqueous solutions so that a destructive method can be applied. Ionic strength and temperature effects will be studied to optimize the process.

4.3 Materials and Methods

Compounds Used PFOS was obtained as heptadecafluorooctane sulfonic acid (Aldrich, St. Loius, MO) and heptadecafluorooctane sulfonic acid potassium salt (Fluka, Steinheim, Switzerland). PFBS was obtained as nonafluorobutane-1-sulfonic acid and nonafluorobutane-1-sulfonic acid potassium salt (Aldrich, St. Loius, MO).

Solution Preparation The PFOS and PFBS solutions were prepared in 6 liter glass Erlenmyer flasks using either ultrapure water or a 10 mM $NaClO_4$ background electrolyte solution. Spiking solutions were prepared by adding 1200 mg of PFOS or PFBS to each flask and equilibrated over night while stirring.

Screening Tests The adsorbent screening tests were performed by adding different amounts of the adsorbents from Table 4-1 to 100 mL of the PFOS and PFBS solutions to 250 mL amber glass jars (Fisher Scientific, Houston, TX). The jars were shaken and allowed to equilibrate at temperatures of 22.5, 38.5, 48, and 58 $^{\circ}$C. The jars were shaken again and allowed to equilibrate for another 24 hours. After 48 hours 25 mL samples were taken and tested for PFOS or PFBS concentrations.

Kinetic Experiments Kinetic experiments were performed for the GAC-F400 and IRA-458 to determine the required time to reach adsorption equilibrium. PFOS and PFBS solutions in 10 mM $NaClO_4$ with initial concentrations of 0.35 mM and 0.55 mM respectively were prepared and placed in 6-liter flasks. The experiments commenced by adding 10 grams of one adsorbent to each flask. The flasks were stirred continuously at 200 rpm and sampled over time to determine solution phase concentrations of PFOS or PFBS.

Isotherm Experiments Two types of isotherm tests were performed. In one testing protocol, different amounts of adsorbent were added to 250 mL amber glass jars containing 100 mL of either PFOS or PFBS solutions in Milli-Q water. The jars were periodically shaken and allowed to equilibrate at temperatures of 22.5, 38.5, 48, and 58 °C for 48 hours. After 48 hours 25 mL samples were taken and tested for PFOS or PFBS concentrations.

Symbols in Figure 4-1	Adsorbent	Type	Particle diameter	Surface Area	Source
NA	CBV-280-14 (ZSM5-280)	hydrophobic zeolite	~1 μM	400 m2/g	Zeolyst International (Kansas City, KS)
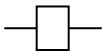	CBV-780 (NaY80)	hydrophobic zeolite	~1 μM	780 m2/g	Zeolyst International (Oosterhorn, Netherlands)
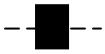	Dowex Monosphere 66	Adsorption Resin	450-550 μm	N/A	Supelco (Bellefonte, PA)
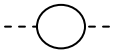	Amberlite IRA-458	Ion Exchange Resin	<1.90 mm	N/A	Supelco (Bellefonte, PA)
	GAC F400	Granular Activated Carbon	0.55 - 0.75 mm	N/A	Calgon (Pittsburgh, PA)
	Dowex Optipore V493	Adsorbent	350-800 μm	1000 m^2/g	Supelco (Bellefonte, PA)
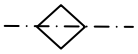	Sepabeads SP-207	Adsorbent	500 μm	650 m^2/g	Supelco (Bellefonte, PA)

Table 4-1: Adsorbents and ion exchange resins tested in the screening test as a potential method of concentrating PFOS and PFBS.

The second type of isotherm test consisted of adding 10 g of adsorbent to 6 L of 10 mM $NaClO_4$ solution. The solutions were continuously stirred at 200 rpm at constant temperatures of 3, 22 and 35 °C. The solutions were then spiked with 200 mg of either PFOS or PFBS. Aqueous samples were taken after 48 hours and the solutions were then

spiked with another 200 mg of either PFOS or PFBS. The sampling and spiking procedure was repeated up to 10 times in order to generate the isotherms.

Solubility Studies Experiments were performed to determine the aqueous solubility of PFOS and PFBS in Milli-Q water and in 10 mM $NaClO_4$ solutions. About 180 mg of PFOS in the acid form or potassium salt were added to 100 mL of water ensuring that enough PFOS would precipitate out of the water when equilibrated. Solutions were mixed for an hour and allowed to equilibrate overnight at temperatures of 4, 22, 40 and 50 $^{\circ}$C. Liquid samples were taken making sure that solids were not removed with the liquid and samples were tested for PFOS concentrations.

Regeneration Studies Regeneration experiments for the IRA-458 were performed using different concentrations of NaCl or NaOH solutions at temperatures of 7, 22, and 50 $^{\circ}$C. Resin loaded with PFOS or PFBS were packed in 1 cm diameter by 10 cm long glass columns (VWR, West Chester, PA). The regenerant solutions were then circulated at 20 mL/min through the columns using a peristaltic pump for 12 hours. Solutions were then sampled for PFOS or PFBS concentrations.

Sample Analysis Two methods were used to determine aqueous phase concentrations of PFOS and PFBS. Concentrations greater than 1 mg/L were determined using a Dionex (Sunnyvale, CA) ICS-3000 ion chromatograph (IC) with a conductivity detector. Mixtures of 20 mM boric acid and 95% acetonitrile in water were used as the mobile phase. PFOS and PFBS were measured using the same procedure as in Chapter 2. Concentrations below 1 mg/L were determined using a Shimadzu model VSH TOC

analyzer (Columbia, MD). The TOC method was verified by comparing it to the IC method for concentrations above 1 mg/L.

The isosteric heats of adsorption were calculated using the data from the PFOS and PFBS isotherms and the van't Hoff equation:

$$\Delta H = R \frac{d \ln C_{aq}}{d \frac{1}{T}} \quad (4\text{-}1)$$

where ΔH is the heat of adsorption (J/mol), C_{aq} is the aqueous concentration at different loadings (mg/L), R is the universal gas constant (8.314 J/mol K) and T is the temperature (K).

4.4 Results and Discussion

Figure 4-1 shows the results from the screening tests which indicated that the GAC-F400 was the most effective adsorbent. Kinetic experiments were then performed on the GAC and the IRA-458 ion exchange resin to determine the approximate time required to reach adsorption equilibrium. Figure 4-2 shows the concentrations of PFOS and PFBS as a function of elapsed time in continuously stirred 6-L flasks containing 10 grams of adsorbent or ion exchange resin. The data for PFOS and PFBS indicate that the equilibration time for the IRA-458 was less than 10 hours, as compared to approximately 50 hours for the GAC-F400.

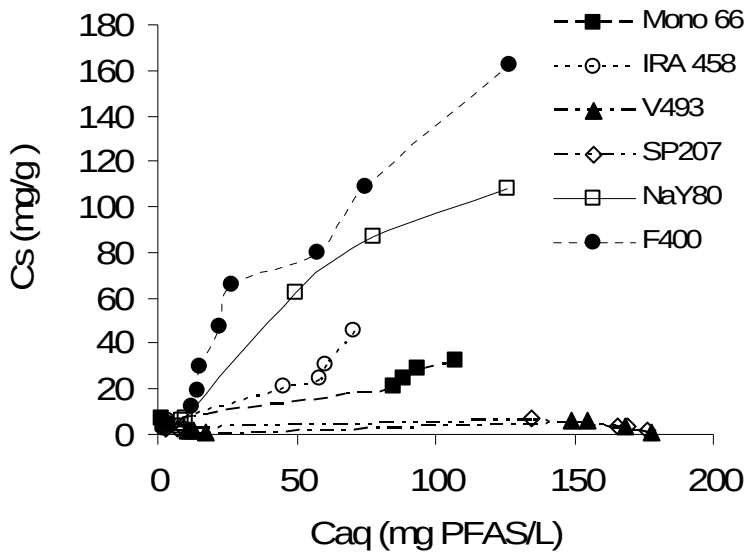

Figure 4-1: PFOS uptake isotherms for several adsorbents at 22 °C. Mono 66 is Dowex Monosphere 66, IRA-458 is Amberlite IRA-458, V493 is Dowex Optipore V493, SP207 is Sepabeads SP-207, NaY80 is CBV-780, and F400 is granular activated carbon (GAC) F400.

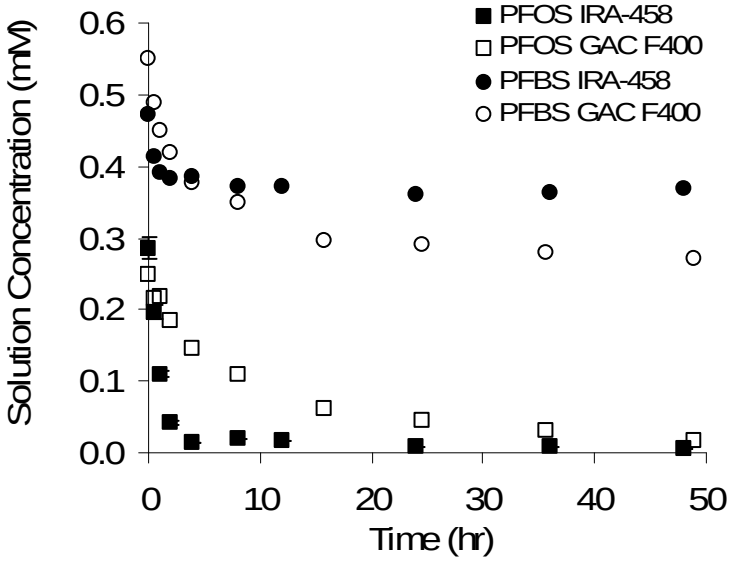

Figure 4-2: Comparison of PFOS and PFBS adsorption on IRA-458 and GAC F400 in a 10 mM $NaClO_4$ solutions.

Isotherm Experiments Isotherms for PFOS and PFBS on the GAC F400 in ultrapure water are shown in Figures 4-3a and b. All the isotherms are highly non-linear and do not readily conform to standard isotherm models. The isotherms show that the PFOS had a higher loading than the PFBS which can be attributed to the differing alkyl chain length. Studies have shown that surfactants with longer alkyl chain lengths tend to adsorb to carbon at higher loadings than their shorter counterparts (*107*). Figure 4-3b shows a leveling off and then an upward trend for PFBS suggesting that the monolayer for PFBS adsorption was reached and multilayer adsorption was taking place. Figure 4-3a did not show this trend because the monolayer coverage was not reached before the end of the experiment. The isotherms for both compounds are very steep at low concentrations indicating that there are a limited number of adsorption sites with very favorable adsorption energies.

Isosteric heats of adorption were used to determine the driving force for the adsorption onto the GAC. For PFOS, isosteric heats of adsorption were calculated for adsorbed phase concentrations between 25 and 150 mg/g and for PFBS isosteric heats were calculated for concentrations between 25 and 50 mg/g. The heats of adsorption for PFOS and PFBS are shown in Figure 4-4. For all loadings, the heats of adsorption for both compounds are endothermic or positive. This indicates that adsorption was promoted by the increase in entropy associated with removing the compound from solution. This effect is called the hydrophobic effect (*108*) and contrasts with the behavior of uncharged hydrophobic organic compounds whose adsorption by activated carbon is promoted by enthalpic effects (*109*). The hydrophobic component of

surfactants, dissolved in an aqueous solution, will partition more favorably to a hydrophobic environment (*110*). Positive enthalpies of adsorption are often observed for surfactants on activated carbon because the carbon itself tends to be hydrophobic. The positive enthalpies arise from removing charged compound, and their counter ions, from aqueous solution (*108*).

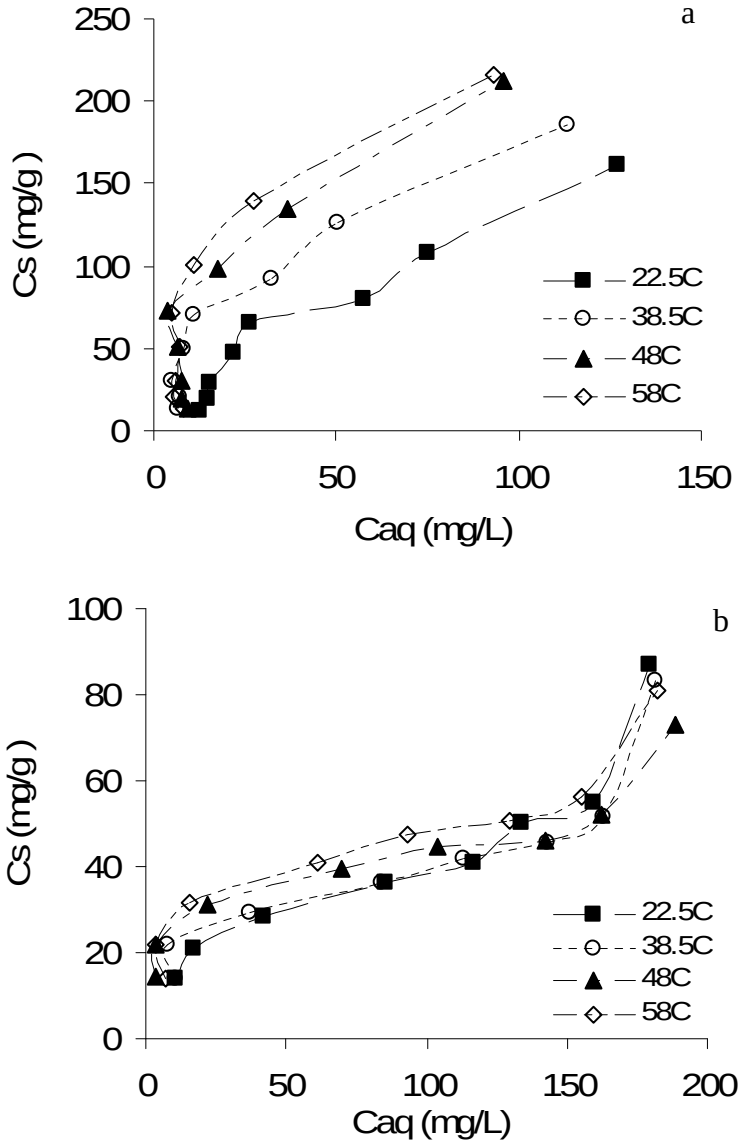

Figure 4-3: a). PFOS and b). PFBS adsorption onto GAC F400. Isotherms were performed in solutions of PFOS or PFBS and water at temperatures ranging from 22.5 to 58 °C.

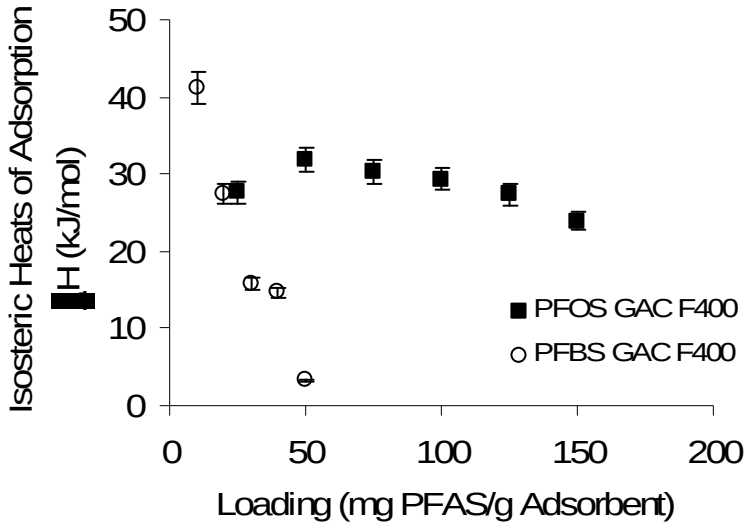

Figure 4-4: Isosteric heats of adsorption of PFOS and PFBS for GAC F400 in pure water for different loadings of PFOS and PFBS.

Isotherms for PFOS and PFBS on the IRA-458 are shown in Figures 4-5a & b. The unusual shape of these isotherms may be attributed to an experimental artifact associated with the differing amounts of resin and PFOS or PFBS added to each flask. Flasks with greater amounts of PFOS or PFBS added had higher ionic strengths. As discussed in the next section, the ionic strength had a significant impact on the solubility of PFOS. The isosteric heats of adsorption for the isotherms in Figure 4-5 are shown in Figure 4-6. Similar to the heats of adsorption for the activated carbon, the heats of adsorption are endothermic. This indicates that solute hydrophobicity may be promoting uptake by the resin more than ion exchange. The increasing heats of adsorption with increasing loading may therefore result from the increasing ionic strength of the solutions with increasing adsorbate concentration. The effect of solute hydrophobicity will increase with increasing ionic strength due to the salting out effect (*111*).

Solubility Studies Solute hydrophobicity can be assessed by measuring its aqueous solubility. The solubility of PFOS in solutions of different ionic composition was determined over a temperature range of 22.5 to 38 °C. The solubility of PFOS has been reported as 370 mg/L and 570 mg/L for fresh water and pure water respectively (*112*) and 498-680 for the potassium salt (*113*). The data in Figure 4-7 show that, while temperature slightly affects the solubility, the ionic strength has a major impact on solubility of PFOS. The data also shows that the different forms of PFOS have different solubility. Studies have shown PFOS to be such a strong anion that it can form strong ion pairs with many cations (***Error! Bookmark not defined.Error! Bookmark not defined.***) which lowers the solubility of the compound.

To minimize the effect of ionic strength on the adsorption isotherms, the experiments were repeated in 10 mM $NaClO_4$ background electrolyte solutions. Figure 4-8a and b show the isotherms for PFOS and PFBS. In contrast to the behavior shown in Figure 4-5, PFOS and PFBS uptake increased with increasing aqueous phase concentrations. For PFOS, the uptake exceeded the ion exchange capacity of the resin, which is 1.8 meq/g. A loading of 500 mg of PFOS per gram of adsorbent corresponds to 1 meq/g. The PFOS isotherms show a maximum loading of 2.1 meq/g, indicating an uptake mechanism other than ion exchange. The PFBS isotherms are considerably less steep than those for PFOS, especially at low concentrations. Since both compounds carry the same charge, the large difference in behavior between PFOS and PFBS supports the hypothesis that hydrophobic effects dominate uptake by the resin.

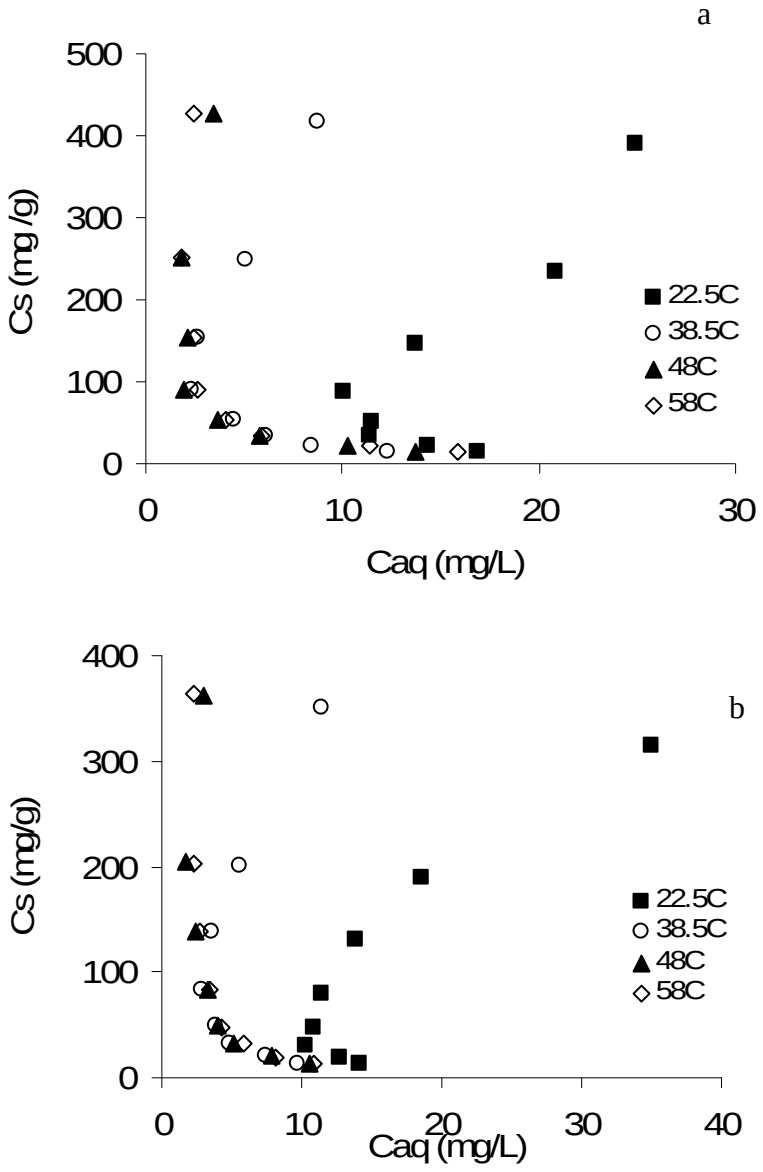

Figure 4-5: a). PFOS and b). PFBS adsorption onto IRA-458. Isotherms were performed in ultrapure water at temperatures ranging from 22.5 to 58 ˚C.

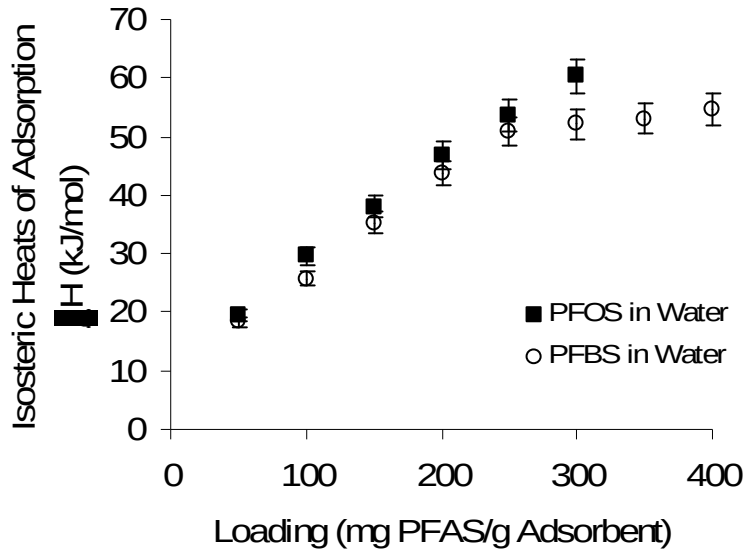

Figure 4-6: Isosteric heats of adsorption for PFOS and PFBS adsorbed onto IRA-458 in ultrapure water.

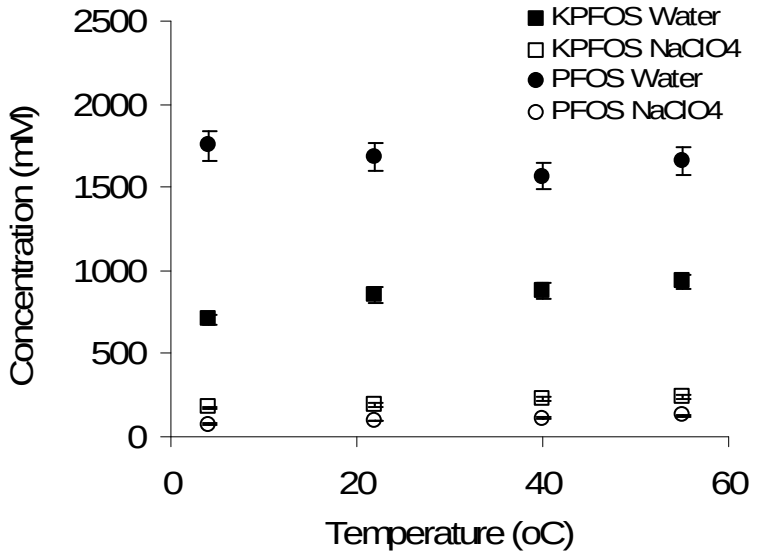

Figure 4-7: Solubility of PFOS in ultrapure water and in 100 mM $NaClO_4$ solutions. KPFOS is the potassium salt of the compound and PFOS refers to the acid form.

Regeneration Studies Experiments were performed to recover PFOS and PFBS from the IRA-458 using NaCl and NaOH solutions of varying concentration. Table 4-2 shows the percentage of PFOS and PFBS that was recovered from the IRA-458 using each regenerant solution. For all concentrations tested, the NaCl solutions did not recover a detectable amount of PFOS. The highest recovery of adsorbed PFOS was achieved using a 320 mM NaOH solution at pH 13. However, only 0.4% of the PFOS was recovered from the resin. Using a 318 mM NaOH solution at pH 13 recovered 4% of the PFBS from the IRA-458.

The low recoveries can most likely be attributed to the low aqueous solubilities of PFOS and PFBS in high ionic strength solutions. Nevertheless, when pure water was used no PFOS was recovered from the resin. This suggests that the adsorption process is not readily reversible.

This study showed that GAC and ion exchange resins can remove PFBS and PFOS from dilute aqueous solutions. The endothermic uptake of both compounds by both adsorbents indicates that thermal regeneration at laboratory conditions will be ineffective. However, more aggressive thermal regeneration, such as that commonly performed on activated carbon, may be effective for these compounds.

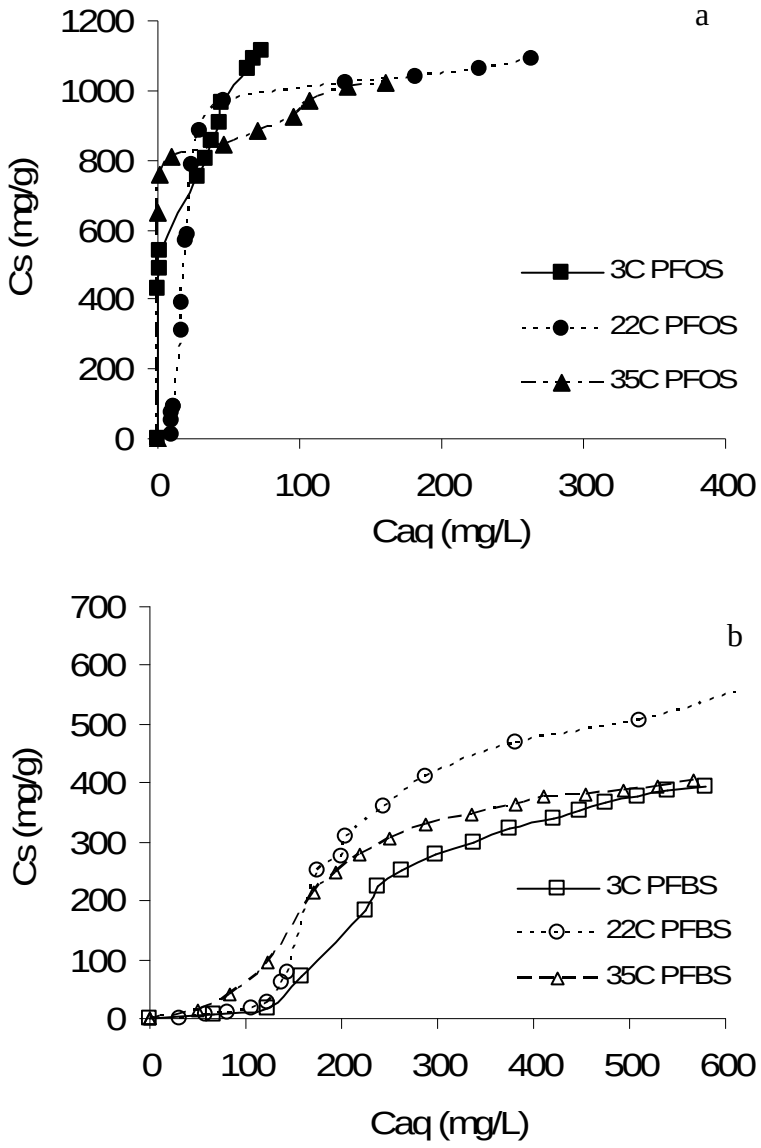

Figure 4-8: a). PFOS and b). PFBS adsorption onto IRA-458. Isotherms were performed in a 10 mM $NaClO_4$ solution and were spiked with PFOS and PFBS. Experiments were performed at temperatures of 3, 22, and 35 $^{\circ}$C.

Compound	Removal Solution	Concentration (mM)	Initial pH	Final pH	Temperature (^{o}C)	% recovered
PFOS	NaCl	32	7.5	4.5	22	ND
PFOS	NaCl	320	7.5	4.5	22	ND
PFOS	NaCl	320	7.5	4.5	50	ND
PFOS	NaCl	320	7.5	4.5	7	ND
PFOS	NaOH	32	12	11.5	22	0.01
PFOS	NaOH	320	13	10	22	0.36
PFOS	NaOH	320	13	13	50	0.18
PFOS	NaOH	320	13	13	7	ND
PFBS	NaOH	320	13	10	22	4.0

Table 4-2: Regeneration of IRA-458 with different solutions and the percent of the PFOS or PFBS recovered. (ND – values were not detected)

4.5 Acknowledgements

Thanks to the National Science Foundation Chemical and Transport Systems Directorate (CTS-0522790), the Semiconductor Research Corporation/Sematech Engineering Research Center for Environmentally Benign Semiconductor Manufacturing (2001MC425), and the Donors of the American Chemical Society Petroleum Research Fund (PRF 43535-AC5) for support of this work.

CHAPTER 5

ELECTROCHEMICAL OXIDATION OF TRICHLOROETHYLENE USING BORON DOPED DIAMOND FILM ELECTRODES

5.1 Abstract

This chapter examines the oxidation of trichloroethene at boron-doped diamond film electrodes. Flow-through experiments were performed to determine the rate of degradation of trichloroethene. The rate of degradation using the flow through reactor was determined to be pseudo-first order and was 0.2539 min^{-1}. Rotating disk electrode experiments were performed at current densities of 2, 4, 8, 12, and 20 mA/cm^2 and were used to determine the effects of current densities while limiting the effects of mass transfer. The rates of reaction appeared to be zeroth order and increased as the current density increased. However, experiments performed at constant current and varying concentration showed that at higher current densities the mechanism was first order with respect to the TCE concentration. Temperature experiments were performed to determine the apparent activation energy. Apparent activation energies of 5.8 kJ/mol and 22.1 kJ/mol at 2 mA/cm^2 and 20 mA/cm^2 respectively show that the mechanism is limited by the mass transfer of the TCE to sites on the electrode surface. Density functional theory studies were completed to determine the mechanism. Comparing the data from the density functional theory and from the apparent activation energy calculated the mechanism for TCE oxidation is controlled by both direct electron transfer and oxidation via hydroxyl radicals. Energy and cost analysis were performed to determine the operating costs for a 25 cm^2 electrochemical reactor. The cost to degrade

500 mg/L of TCE to 1 mg/L was $44.00. For every decade decrease in effluent concentration the cost increased by $16.00.

5.2 Introduction

Trichloroethene (TCE) is a chlorinated organic solvent and is used as a degreasing agent, dry cleaning solvent, and chemical extraction agent in a variety of industries (*114, 115*). Past disposal practices and spills have made trichloroethene a major contaminant in groundwaters, soils, and sediments (*116*). TCE may cause liver damage and failure of the central nervous system and is considered a likely carcinogen. Considered a toxin and carcinogen, the US Environmental Protection Agency (EPA) has established the maximum contaminant level for TCE in drinking water at 0.005 mg/L.

The most common way of treating TCE in aqueous systems includes the use of air stripping and followed by adsorption onto granular activated carbon (GAC) (*117*). Air stripping displaces TCE into the gas phase. Once in the gas phase the TCE is usually adsorbed onto a GAC bed. This method is very effective in the removal of TCE from water but the possible release of volatile organics into the atmosphere is a concern. The problem of other volatile organic compounds, which compete with TCE for sites on the activated carbon, can limit the effectiveness of the GAC. The used GAC requires the regeneration of the GAC off site, which is costly, and a concentrated waste stream of TCE must then be properly disposed (*118, 119*).

Combustion and oxidation of TCE using metal catalysts have been established as effective methods for degrading TCE. These catalysts are expensive but can provide

selectivity for total oxidation products and reaction conditions (*120 - 122*). Platinum, palladium, ruthenium, and rhodium have shown to be highly effective in the degradation of TCE. However, high temperatures are needed and groundwater conditions may deactivate these catalysts. These methods also produce chlorinated by-products and Cl_2, which can lead to the deactivation of these catalysts (*121*).

Oxidation using O_3/H_2O_2, UV/H_2O_2, and sonochemistry have been successful at removing TCE in groundwater and reclaimed water (*123 - 130*). These studies have shown that TCE is degraded through both oxidation via hydroxyl radicals and direct UV photolysis in less than 10 minutes. The major byproducts were formic, oxalic acids, and chloride ions. $UV/TiO_2/O_3$ offers fast kinetics in removing TCE (*131*). However, in most aqueous systems there are other compounds, such as carbonate and bicarbonate, that act as scavengers for the hydroxyl radicals slowing down the degradation of TCE and other chlorinated organic compounds. More readily oxidized compounds will use up the ozone and H_2O_2 before TCE can be degraded. These methods require the use of costly UV lamps, TiO_2 catalysts, production of ozone and/or large quantities of hydrogen peroxide.

The addition of oxidizing compounds has proven to be an appealing process for degrading TCE in aqueous systems. Compounds such as permanganate and persulfate, and heat activated persulfate react quickly with TCE (*132 - 137*). These methods degrade TCE to dichloroethene (DCE) and other chlorinated organics, as well as chloride ions. Nevertheless, the reactions are pH and concentration dependent. In the case of heat activated persulfate, high temperatures between 250 to 350^{o}C are required (*137*).

Electrochemical oxidation can overcome the limited oxidizing abilities of conventional AOPs, since potentials on the electrodes can be made much more oxidizing than hydroxyl radicals. Electrochemical systems provide an inexpensive method for treating water contaminated with organic solvents and surfactants. Electrochemical reduction of TCE using iron, palladized-iron and mixed metal oxide-coated titanium mesh electrodes has been a successful method for degradation of TCE (*138, 139*). The major reductive products included chlorine, ethane, ethene, acetylene, chloride ions. Electrochemical oxidation of TCE using an electrically conductive ceramic anode (Ti_4O_7) was shown to be independent of pH and the final products were CO_2, CO, Cl^- and ClO_3^- (*115*). However, these electrodes can oxidize water which can compete with TCE oxidation. Other dimensionally stable electrodes, such as titanium coated with various catalysts, are prone to fouling (*140*). Noble metals, such as platinum, are stable when used as anodes and cathodes, but they have high catalytic activity for water electrolysis. These electrodes are prone to fouling by chemically adsorbed compounds (*141, 142*).

In order for application of an electrochemical system to be successful, the electrodes must retain their structural integrity over a range of potentials and remain reactive for extended periods (*139*). Boron-doped diamond film electrodes can overcome these difficulties because of their high anodic stability, low catalytic activity for water electrolysis, and effectiveness (*141, 143*). These electrodes resist fouling by containing no catalysts. So they are good candidates for electrochemical oxidation treatment of contaminated waters and have been studied for use as anodes in water treatment applications (*144 - 146*). This research investigated the effectiveness of boron-doped

diamond (BDD) film electrodes for oxidizing TCE in dilute aqueous solutions. Boron-doped diamond film electrodes have been shown to oxidize organic surfactants through direct electron transfer. Reaction rates and reaction products were measured in both flow-through and rotating disk electrode reactors. The effects of current density and concentration on reaction rates were determined. Quantum mechanical simulations using density functional theory (DFT) were used to evaluate potential energy barriers associated with the oxidation of TCE.

5.3 Materials and Methods

Rotating Disk Electrode Reactor Experiments measuring TCE oxidation rates were performed in a two chamber glass cell separated into anodic and cathodic compartments, with solution volumes of 250 mL and 60 mL respectively. The compartments were separated by a Nafion membrane (Fuel Cell Scientific, Stoneham, MA). The working electrode consisted of a 1.1 cm diameter disk composed of a BDD film on a p-silicon substrate (Adamant Technologies, Neutchatel, Switzerland). The disk electrode was operated using a Princeton Applied Research (PAR) (Oak Ridge, TN) rotating disk electrode (RDE) assembly. The electrode was rotated at 3000 revolutions per minute to eliminate mass transfer limitations on the measured reaction rates. The counter electrode was a 30.5 cm long by 0.6 cm diameter graphite rod, and an Hg/Hg_2SO_4 electrode saturated with K_2SO_4 served as the reference. Currents and electrode potentials were controlled using a PAR model 273A potentiostat. All potentials were corrected for

uncompensated solution resistance and are reported with respect to the standard hydrogen electrode (SHE) by adding 0.64 V to the Hg/Hg_2SO_4 electrode potentials.

Experiments were performed over a temperature range of 2 to $42^{O}C$ in 16 mM K_2SO_4 background electrolyte solutions with an initial pH value of 10.5. The experiments were performed at constant TCE concentrations of 0.98, 1.7, 3.6 and 5.4 mM by purging the solution in the anode chamber with 50 mL/min of nitrogen gas containing TCE at different concentrations. The solution in the anode chamber was sampled at 20 minute intervals and TCE oxidation rates were determined from the reaction product concentrations. Solution pH values were measured using pH-indicator strips (Fisher Scientific, Pittsburgh, PA) calibrated in 0.2 pH units.

Flow Through Reactor Because the RDE reactor was open to the atmosphere through the electrode shaft opening, a MiniDiacell® (Adamant Technologies) gas-tight, flow-through reactor was used to determine the TCE reaction products. The flow-through reactor contained one bipolar and two monopolar electrodes composed of the same BDD films on p-silicon that were used in the RDE reactor. The electrodes were 5 cm long and 2.5 cm wide and the bipolar electrode was situated between the two monopolar electrodes with an inter-electrode gap of 3 mm. The two anodes in the cell provided a total anodic surface area of 25 cm^2. The cell had a solution capacity of 15 mL, which yielded a surface area to volume ratio of 1.67 cm^{-1}. The monopolar electrodes were connected to a Protek (Stayton, OR) model 3050 direct current power supply. The flow-through cell was operated galvanostatically and no reference electrode was used.

The flow-through reactor was operated in a closed-loop system consisting of a 1.2 L liquid chromatography reservoir and a liquid chromatography pump connected via Teflon® tubing. Experiments were performed by recirculating 1 L of a solution containing 1.6 mM TCE and 16 mM K_2SO_4 background electrolyte at a rate of 10 mL/min. The reservoir was connected to a pressure gauge via a 0.635 cm (o.d.) stainless steel column containing a palladium catalyst (Aldrich). The catalyst was used to promote H_2 oxidation to water in order to prevent pressure build-up from the gases produced from water electrolysis. The solutions were sampled over time to determine TCE and reaction product concentrations. To account for only the time that the fluid spent in the reactor, the elapsed electrolysis times were calculated from:

$$\text{electrolysis time} = \text{elapsed real time} \times \frac{\text{reactor volume}}{\text{fluid volume in reservoir}} \qquad (5\text{-}1)$$

Product Analyses Headspace samples from the flow-through system were taken with gas-tight syringes and were analyzed for volatile products using gas chromatography/mass spectrometry (GC/MS) and aqueous samples were analyzed for nonvolatile products using liquid chromatography/mass spectrometry (LC/MS). These analyses were performed by the University of Arizona, Department of Chemistry Mass Spectrometry Facility. Aqueous samples from the flow-through reactor were analyzed for volatile reaction products via extraction into 1 g of pentane followed by gas chromatography analysis using an electron capture detector. Aqueous samples from the RDE reactor were analyzed for nonvolatile reaction products using a Dionex IC-3000 ion chromatograph equipped with an electrical conductivity detector and an Ion Pac AS18 column (4 x 250 mm) with an AG18 pre-column (4 x 50 mm). Mobile phase was generated using an

EGCII KOH EluGen cartridge that produces potassium hydroxide at a concentration of 20 mM.

Quantum Mechanical Simulations Density functional theory (DFT) simulations were performed to calculate the activation barriers for different possible TCE reaction mechanisms. DFT calculations were performed using the DMol3 (*147*, 148) package in the Accelrys Materials Studio (*149*) modeling suite using a personal computer operating with a 2.8 GHz Pentium 4 processor. All simulations used double-numeric with polarization (DNP) basis sets (*150*) and the gradient corrected Becke-Lee-Yang-Parr (BLYP) (*151*, *152*) functional for exchange and correlation. The nuclei and core electrons were described by DFT optimized semi-local pseudopotentials (*153*). Implicit solvation was incorporated into all simulations using the COSMO-ibs (*154*) model.

Transition state searches were performed using a quadratic synchronous transit (QST) method (*155*) and refined using an eigenvector following method (*156*). The energy optimized structures and transition states were verified by frequency calculations. Imaginary frequencies with wave numbers smaller than 30 cm^{-1} were considered numerical artifacts of the integration grid and convergence criteria (*157*, *158*).

5.4 Results and Discussion

Figure 5-1 shows the aqueous TCE concentration as a function of electrolysis time in the flow through reactor operated at a current density of 20 mA/cm^2. TCE degradation was first-order in TCE concentration with a pseudo-first order rate constant (k_1) of 3.94 $\pm$ 0.20 min^{-1}. Because the flow-through reactor did not contain a membrane

separating the anodic and cathodic chambers, TCE degradation in Figure 5-1 can be attributed to both oxidation and reduction.

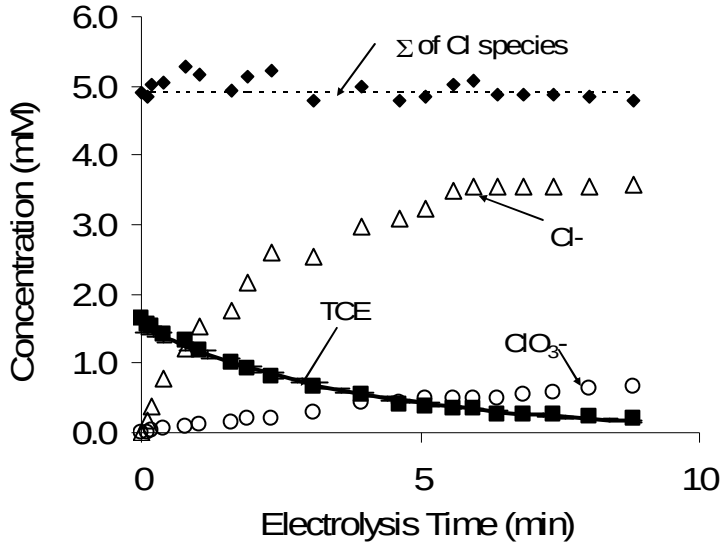

Figure 5-1: Electrochemical oxidation of TCE in a flow through reactor as a function of electrolysis time. TCE oxidation is first order at BDD electrodes. ΣCl is the sum of the chlorine species, which shows almost all of the chlorines removed from TCE were accounted for.

The TCE degradation products in the flow through reactor were formate, acetate, chlorate, chloride, and carbon dioxide. Because TCE reduction at BDD cathodes produced only acetate and chloride ions (*124*), the formate, chlorate, and carbon dioxide are exclusively anodic reaction products. Figure 5-1 also shows the mass balance for chlorine, which is equal to the sum of 3 times the molar TCE concentration plus the molar concentrations or chloride and chlorate. Throughout the course of the electrolysis period, the three chlorine containing species, TCE, Cl^- and ClO_3^- accounted for close to 100% of the chloride balance, confirming the absence of any measurable concentrations of chlorinated organic intermediates. The absence of detectable chlorinated organic

intermediates cannot be taken as evidence that they are not produced, but may indicate that the intermediates are sufficiently fast reacting that they do not accumulate in the bulk solution.

TCE reaction rates were determined in the RDE reactor based on chloride and chlorate ion generation rates in the anodic chamber of the reactor. Figure 5-2 shows the sum of the Cl^- and ClO_3^- concentrations (ΣCl) as a function of electrolysis time for solutions containing TCE at a fixed concentration of 3.8 mM. Figure 5-3 shows the same behavior at a TCE concentration of 1.7 mM. Over the entire range of current densities and TCE concentrations investigated, there was a linear increase in ΣCl with electrolysis time, indicating that the reaction products did not compete with TCE for reactive sites on the electrode surface. At the lowest current density investigated (2 mA/cm^2), formate was stoichiometrically produced from TCE oxidation and no acetate production was observed. At higher current densities, formate and acetate concentrations were always less than 50% of the TCE that was degraded. The buildup of formate in the experiments at 2 mA/cm^2 can be attributed to its much slower reaction rate as compared to TCE. In separate experiments, formate oxidation rate was the same as that for TCE and a current density of 20 mA/cm^2, but were 2 times slower at a current density of 2 mA/cm^2. The low concentration of formate in the experiments conducted at higher current densities suggests that formate is degraded at the same time that TCE is degraded.

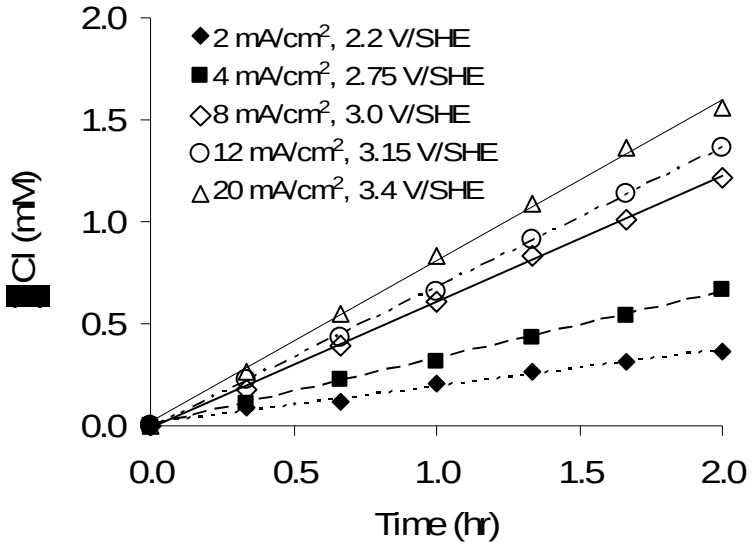

Figure 5-2: Electrochemical oxidation of TCE in a RDE reactor as a function of time for 3.80 mM of TCE in solution. The k values for 2, 4, 8, 12, and 20 mA/cm^2 were 0.1787, 0.3296, 0.6160, 0.6838, and 0.7920 mM/hr, respectively.

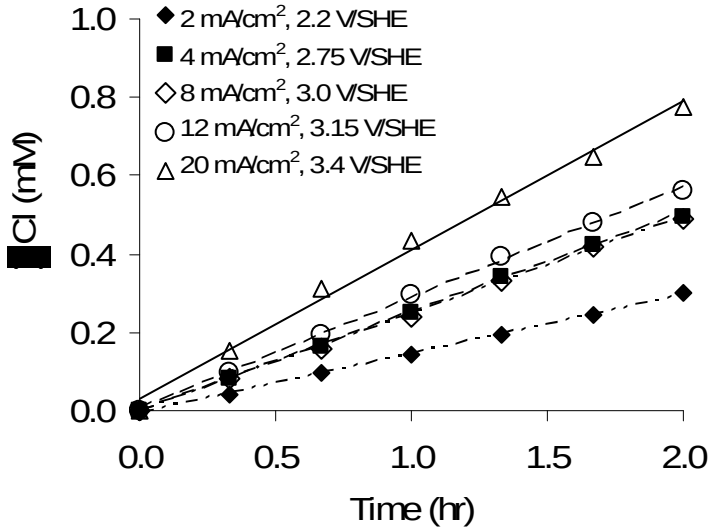

Figure 5-3: Electrochemical oxidation of TCE in a RDE reactor as a function of time for 1.7 mM of TCE in solution. The k values for 2, 4, 8, 12, and 20 mA/cm^2 were 0.1506, 0.2518, 0.2479, 0.2840, and 0.3806 mM/hr, respectively.

Figure 5-4 shows the rates of TCE oxidation as a function of the aqueous TCE concentration for current densities of 2 and 20 mA/cm^2. At a current density of 2 mA/cm^2, the TCE reaction rate was independent of the TCE concentration, thereby exhibiting reaction kinetics that were zeroth-order in TCE concentration. In this circumstance, TCE oxidation rates were limited by the electrode current. In contrast, at a current density of 20 mA/cm^2, the TCE reaction rate increased linearly with TCE concentration, thereby exhibiting reaction kinetics that were first order in TCE concentration. Under these conditions, TCE removal rates were controlled by the rate-limited step for TCE oxidation. Based on a solution volume of 250 mL and an electrode surface area of 1 cm^2, the data at 20 mA/cm^2 yield a surface area normalized pseudo first-order rate constant (k_1^{sa}) of 3.3 cm/min. This value is 40% greater than the k_1^{sa} of 2.36 cm/min calculated for the data in Figure 5-1, and indicates that the TCE destruction rates in the flow-through reactor (which include both oxidation and reduction) were mass transfer limited.

Figure 5-5 shows the Faradaic current efficiency, defined as the fraction of the cell current going towards TCE oxidation, as a function of the current density for TCE concentrations of 1.7 and 3.8 mM. At a current density of 2 mA/cm^2, TCE oxidation accounted for more than 50% of the cell current for both TCE concentrations. With increasing current density, the Faradaic current efficiency decreased due to greater rates of oxygen evolution with increasing current density.

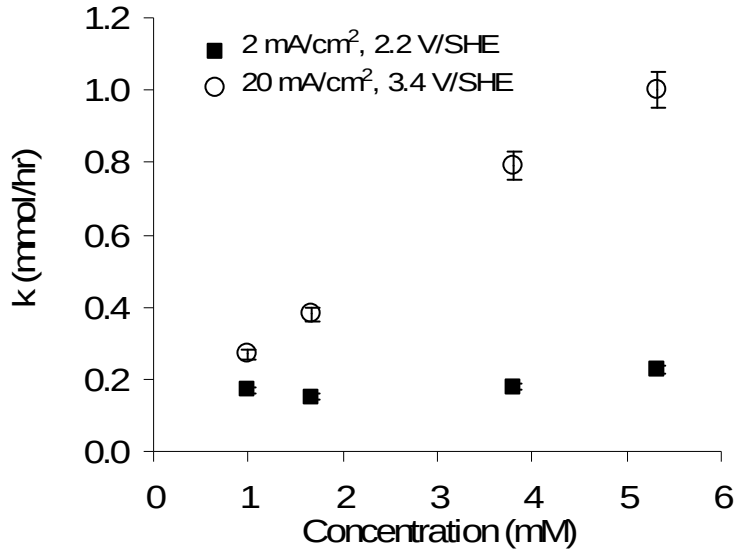

Figure 5-4: Rate constants, k_0 or k_1, as a function of TCE concentration for 2 mA/cm^2 and 20 mA/cm^2.

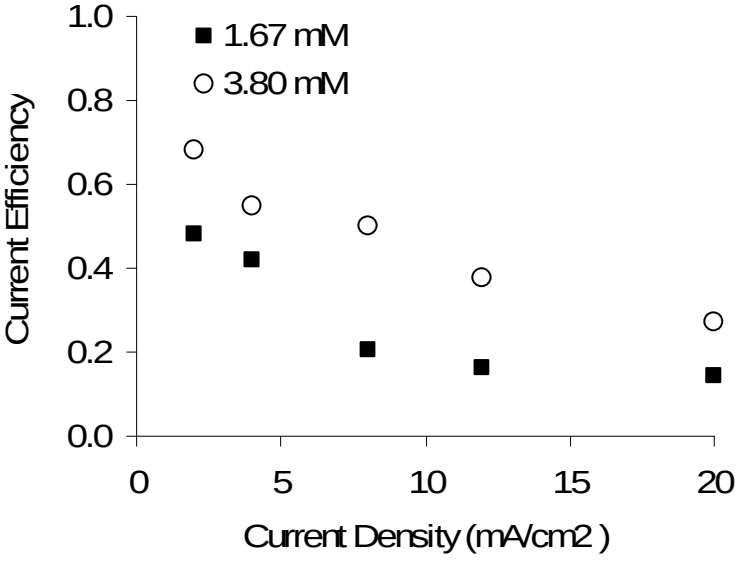

Figure 5-5: Current efficiency as a function of current density. Current efficiency decreases as the current density increases.

Several lines of evidence indicate that the rate-limiting mechanism for TCE oxidation is a function of the electrode potential. The apparent activation energy (E_a) can be used to gain insight into the rate-limiting mechanism for TCE destruction. The E_a values were determined at fixed electrode potentials of 2.2 and 3.4 V/SHE by measuring reaction rates at 2, 22 and 42° C. At 2.20 V, the apparent activation energy was 5.8 ± 0.3 kJ/mol and at 3.50 V an Ea value of 22.1 ± 1.1 kJ/mol was measured. These values can be compared to activation barriers calculated by DFT for different reaction mechanisms.

DFT Simulations The activation energy for oxidation of TCE via a direct electron transfer mechanism was determined by calculating the E_a associated with the loss of 1 electron from the highest occupied molecular orbital (HOMO). DFT simulations on the uncharged, solvated TCE molecule showed that the HOMO was associated with the C-H bond. Therefore, the C-H bond was taken as the reaction coordinate and the E_a as a function of the electrode potential was calculated for the reaction:

$$CCl_2CClH \rightarrow CCl_2CCl^{\bullet} + H^+ + e^- \qquad (5\text{-}2)$$

using the method of Anderson and Kang (*159*). The reactant energies were calculated by varying the length of the C-H bond from its minimum energy length of 1.76 Å, followed by geometry optimization of the structure. The product energies were calculated using the atomic positions determined from the optimized reactant structures, followed by self-consistent field optimization of the electronic configurations. Electron energies from the vacuum scale were converted to the SHE scale by subtracting 4.6 eV (*154*). Product energies as a function of electrode potential were determined by shifting the energy profile of the product species downwards by 96.5 kJ/mol (*i.e.*, 1.0 eV) to increase the

electrode potential by 1.0 V and upwards by 96.5 kJ/mol to decrease the electrode potential by 1.0 V (*154*). Intersection of the product and reactant energy profiles yields the bond length of transition state and the activation energy for the reaction, as illustrated in Figure 5-6a. The higher the electrode potential, the shorter the C-H bond stretching required for the reactant and product energy profiles to intersect. By shifting the products energy profile up and down, activation energies as a function of electrode potential were calculated, as shown in Figure 5-6b.

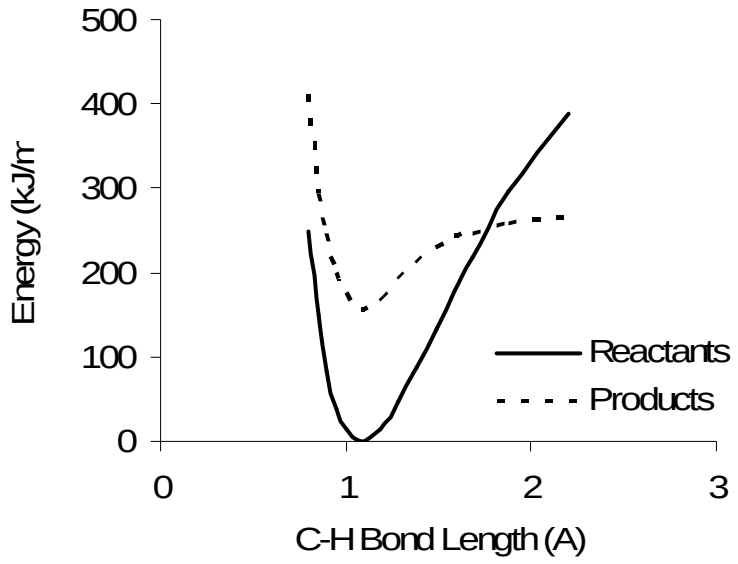

Figure 5-6a: Energy as a function of bond length for the oxidation of TCE. Intersection between the reactants and products provides the activation energy (kJ/mol).

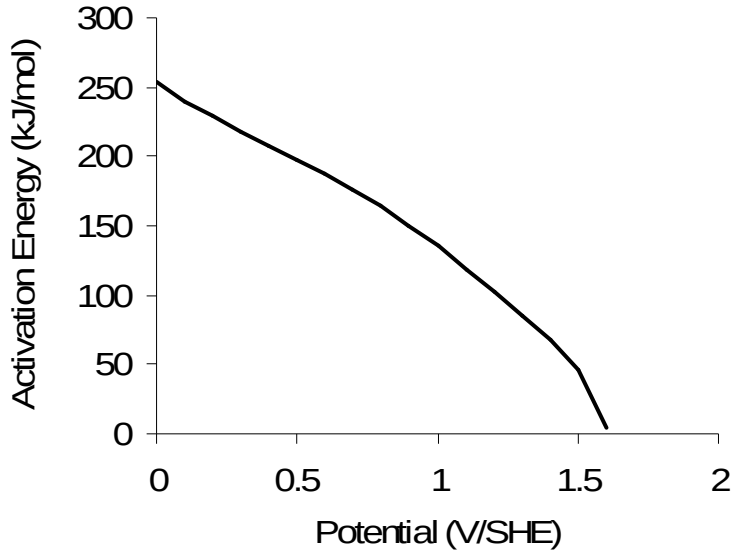

Figure 5-6b: Activation energy versus the bond length for the oxidation of TCE at a BDD anode.

Figure 5-6b shows that the calculated activation barrier for TCE oxidation decreased from 254 kJ/mol at an electrode potential of 0.0 V/SHE to 0 kJ/mol at potentials ≥ 1.6 V/SHE. The experiments performed in this investigation were performed at electrode potentials ranging from 2.2 to 3.4 V/SHE. Therefore, the experiments were performed at sufficiently high overpotentials that direct electron transfer could proceed without any thermal activation (*160*). This indicates that TCE oxidation via direct electron transfer should readily occur in the potential range investigated here. The non-zero E_a of 5.8 kJ/mol may be attributed to second order effects of temperature, such as its effect on diffusion coefficients, the composition and thickness of the electrical double layer at the electrode surface, or the relative adsorption strengths of water and TCE on the electrode surface. Linear sweep voltammetry scans in electrolyte solutions with and

without TCE also support a reaction mechanism involving direct electron transfer. Figure 5-7 shows that currents in solutions containing TCE were greater than those in the blank electrolyte. The greater currents in the TCE containing solutions at potentials where there is very little water oxidation (i.e., E<2.75 V/SHE) can likely be attributed to direct oxidation of TCE. The current peak centered at 2.7 V is consistent with oxidation of TCE adsorbed on the electrode surface at the commencement of the scan. Thus, the data in Figure 5-6 indicate that TCE can be readily oxidized at potentials below those that produce HO radicals from water oxidation.

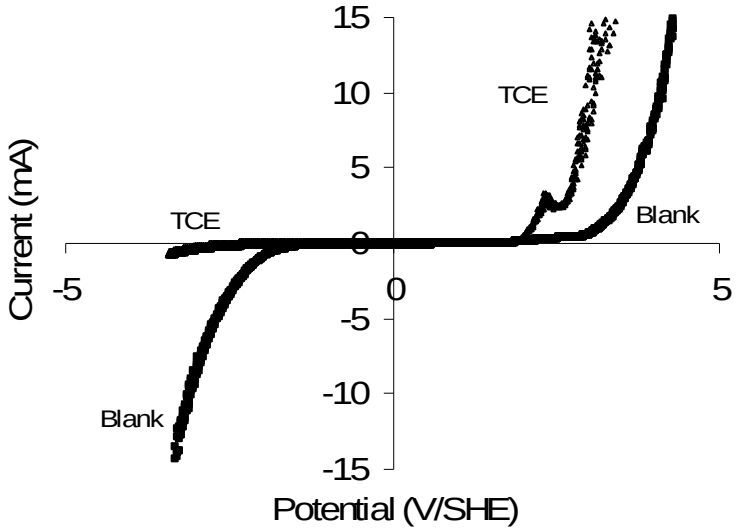

Figure 5-7: Linear scan of current density, i, as a function of potential in an $NaClO_4$ electrolyte solution. Figure shows that as TCE is added to the solution the solvent blocks the oxidation of water.

At higher electrode potentials, the measured E_a value of 22 kJ/mol suggests that HO radicals may also be contributing to indirect TCE oxidation. The activation barriers for attack of $HO^{\cdot}$ radicals at different sites on the TCE molecule were determined using

DFT simulations. The initial reactants configuration for $HO^{\cdot}$ attack at the H atom in TCE are shown in Figures 5-8a. Figure 5-8b and 5-8c shows the transition state and resulting products for the reactants in Figure 5-8a. The overall Gibbs free energy change for this reaction is -30 kJ/mol and the activation barrier is 12 kJ/mol. The low activation barrier suggests that TCE may be readily oxidized by hydroxyl radicals reacting at the H atom. The fact that the calculated barrier is smaller than the E_a of 22.1 ±1.1 kJ/mol measured at 3.4 V/SHE may in part be attributed to the effect of temperature on the rates of HO radical generation. Greater rates of HO generation at higher temperatures would lead to an overestimation of the Ea for TCE oxidation by hydroxyl radicals. This is likely the case since the rate of water oxidation, which produces an HO intermediate, increased by a factor of three between 2 and 42°C. Therefore, the experiments likely give an overestimation of the activation barrier for TCE oxidation by hydroxyl radicals.

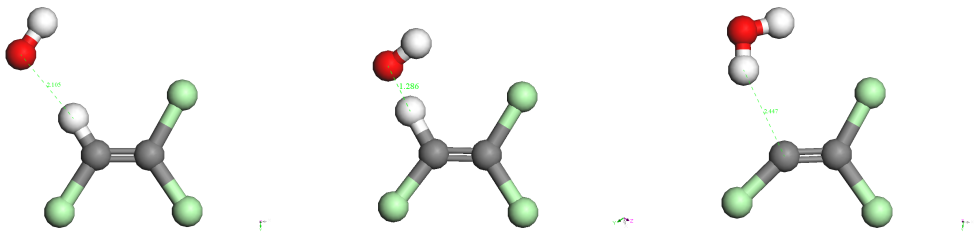

a b c

Figure 5-8: a). Initial reactants for OH attack at the H atom in TCE. b). The transition state and c). resulting products for the reactants in 8a.

Hydroxyl radical attack at the carbon atoms in TCE were also calculated. The initial reactants, transition state and final products at the hydrogen containing carbon atom are shown in Figure 5-9a, b, and c, respectively. The overall Gibbs free energy

change for this reaction is -143 kJ/mol and the activation barrier is 120 kJ/mol. Although the overall energy change is highly exergonic, the high activation barrier indicates that HO attack on this carbon atom should not measurably contribute to the measured reaction rates.

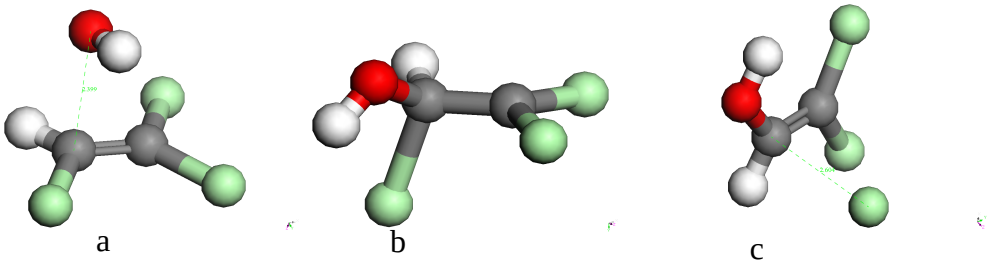

Figure 5-9: Hydroxyl radical attack at the carbon atoms in TCE: a). Initial reactants, b). transition state, c). final products at the hydrogen containing carbon atom.

This study shows BDD electrodes are capable of rapidly oxidizing TCE to inorganic reaction products. The process likely involves both direct oxidation via electron transfer and indirect oxidation via reaction with hydroxyl radicals produced from water oxidation. Although the reaction rates in the flow-through reactor were mass transfer limited, the destruction half-life TCE of less than 3 minutes indicates that the kinetics are sufficiently fast for implementation in a practical treatment system. To minimize the required reactor size, the system would benefit from pre-concentration of the TCE using an adsorbent or membrane. Using the Faradaic current efficiency of 10% and the rate constant determined from the data in Figure 5-1, the electrical power requirements per factor of 10 decreases in concentration are 160 kWhr/1000 gallons for a reactor operating at a current density of 20 mA/cm^2. With electrical costs of $0.10 per

kW-hr, this translates into $16.00 per 1000 gallons per decade decrease in concentration. These calculations are detailed in Chapter 3 and the results are found in Figure 5-10.

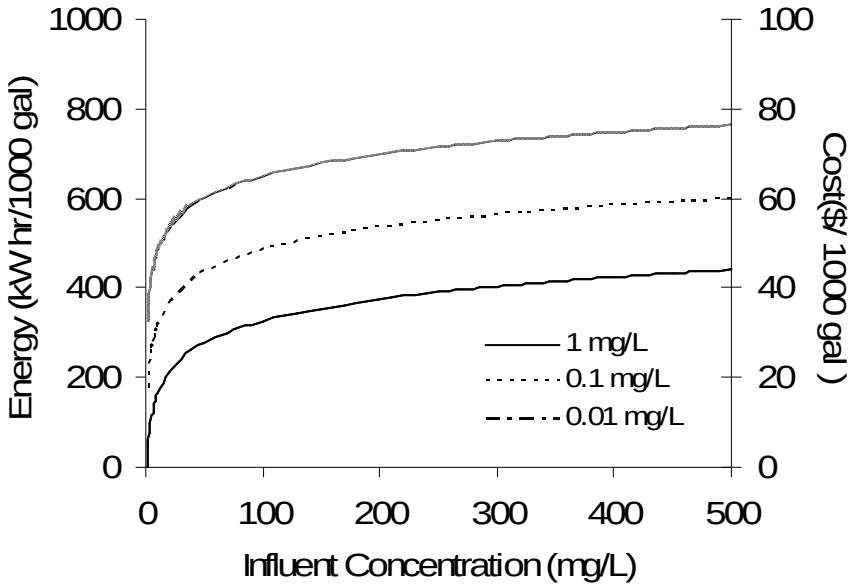

Figure 5-10: Energy and cost analysis for degrading TCE from different influent concentrations to final concentrations of 1 mg/L, 0.1 mg/L and 0.01 mg/L. Energy costs were determined using the first order rate constant from Figure 5-1.

5.5 Acknowledgements

Thanks to the National Science Foundation Chemical and Transport Systems Directorate (CTS-0522790) and to the Semiconductor Research Corporation /Sematech Engineering Research Center for Environmentally Benign Semiconductor Manufacturing (2001MC425) for funding.

CHAPTER 6

CONCLUSIONS AND RECOMMENDATIONS

6.1 Conclusions

The electrochemical oxidation of PFOS and PFBS at boron-doped diamond film anodes is a rapid process with half-lives between 5 to 10 minutes depending on the current density. Products formed from the degradation of these two compounds, such as fluoride and sulfate, can easily be removed using reverse osmosis or ion exchange. With a reaction rate that is 1.5 times smaller than that of PFOS, PFBS requires longer treatment times. The cost to degrade PFBS is 1.5 times higher than that of PFOS. Due to the higher cost and increasing treatment time, PFBS would not be a good replacement for PFOS in industrial uses.

The adsorption of PFOS and PFBS is easily attained using granular activated carbon F400 (GAC F400) and IRA-458. Adsorption onto granular activated carbon increased with increasing temperatures making the GAC F400 difficult to regenerate. Adsorption onto the ion exchange resin was affected by the solubility of the PFOS and PFBS. Increasing the ionic strength of the solution increased the amount of PFOS and PFBS that is adsorbed onto the ion exchange resin and the regeneration of the resins. After trying to regenerate the resins little or no PFOS or PFBS was removed from the resin. Therefore GAC F400 and IRA-458 are good for adsorption of PFOS and PFBS from aqueous systems; however, neither the GAC nor ion exchange resin would be a viable method for concentrating these compounds.

Trichloroethylene (TCE) is quickly degraded using BDD anodes with a half-life of 2.5 minutes. The rate of degradation using the flow through reactor was 0.2539 min^{-1}. TCE oxidation is controlled by both direct electron transfer and oxidation via hydroxyl radicals depending on the potential applied to the electrodes. Energy and cost analysis were performed to determine the operating costs for a 25 cm^2 electrochemical reactor. The cost to degrade 500 mg/L of TCE to 1 mg/L was $44.00. For every decade decrease in effluent concentration the cost increased by $16.00.

6.2 Recommendations

Other processes such as sonication, reductive dehalogenation, and photolysis requires longer treatment times to degrade PFOS and PFBS, electrochemical oxidation seems to be the most appropriate method of degrading these compounds. Further studies should be performed to determine how other compounds in industrial wastewaters affect the degradation of PFOS and PFBS at BDD anodes. Competition between PFOS or PFBS and other compounds for electrode surface may slow down or limit the oxidative degradation of the perfluorinated surfactants.

Studies should be performed on other methods for concentrating PFOS and PFBS. One method may be the use of SPE C18 and then extraction using methanol. The methanol can be evaporated off and the concentrated PFOS can then be electrochemically degraded. However, the affect of other contaminants in the wastewater for the adsorption of PFOS or PFBS will have to be determined. The use of reverse osmosis membranes has been shown to be effective at removing 99% of PFOS from semiconductor

wastewaters. However, the possible degradation of membranes due to other compounds in the aqueous waste streams should be determined.

Studies should be performed on the electrochemical degradation of other chlorinated solvents including carbon tetrachloride and perchloroethylene. If these compounds are readily degradable using BDD anodes, then further studies should be performed to determine the amount of time needed to degrade a mixture of chlorinated solvents. Field studies could be performed on groundwater contaminated with chlorinated solvents.

REFERENCES

(1) Panizza, M.; Delucchi, M.; Cerisola, G. Electrochemical degradation of anionic surfactants. *J. of Applied Electrochem*. **2005**, 35, 357-361.

(2) Lissens, G.; Pieters, J.; Verhaege, M.; Pinoy, L.; Verstraete, W. Electrochemical degradation of surfactants by intermediates of water discharge at carbon-based electrodes. *Electrochim. Acta* **2003**, 48, 1655-1663.

(3) Farrell, J.; Martin, F. J.; Martin, H. B.; O'Grady, W. E.; Natishan, P. Anodically generated short-lived species on boron-doped diamond film electrodes. *J. Electrochem. Soc*. **2005**, 152, E14-E17.

(4) Gandini, D.; Mahe, E.; Michaud, P. A.; Haenni, W.; Perret, A.; Comninellis, Ch. Oxidation of carboxylic acids at boron-doped diamond electrodes for wastewater treatment. *J. App. Electrochem*. **2000**, 30, 1345-1350.

(5) Holt, K. B.; Bard, A. J.; Show, Y.; Swain, G. M. Scanning electrochemical microscopy and conductive probe atomic force microscopy studies of hydrogen terminated boron-doped diamond electrodes with different doping levels. *J. Phys. Chem. B* **2004**, 108, 15117-15127.

(6) Tamilmani, S.; Huang, W. H.; Raghavan, S.; Farrell, J. Electrochemical treatment of simulated copper CMP wastewater using boron-doped diamond thin film electrodes – a feasibility study. *IEEE Trans. Semicond. Manufact*. **2004**, 17, 448-454.

(7) Pastor-Moreno, G.; Riley, D. J. The influence of surface preparation on the electrochemistry of boron-doped diamond: a study of the reduction of 1,4-benzoquinone in acetonitrile. *Electrochem. Comm*. **2002**, 4, 218-221.

(8) Latto, M. N.; Riley, D. J.; May, P. W. Impedance studies of boron-doped CVD diamond electrodes. *Diamond and Related Mater*. **2002**, 9, 1181-1183.

(9) Suffredini, H. B.; Machado, S. A. S.; Avaca, L. A. The water decomposition reactions on boron-doped diamond electrodes. *J. Braz. Chem. Soc*. **2004**, 15, 16-21.

(10) Eingag, Y.; Sato, R.; Olivia, H.; Shin, D.; Ivandini, T. A.; Fujishima, A. Modified diamond electrodes for electrolysis and electroanalysis applications. *Electrochim. Acta* **2004**, 49, 3989-3995.

(11) Panizza, M.; Cerisola, G. Application of diamond electrodes to electrochemical processes. *Electrochim. Acta* **2005**,51, 191-199.

(12) Kraft, A.; Stadelmann, M.; Blaschke, M. Anodic oxidation with doped diamond electrodes: a new advanced oxidation process. *J. Hazard. Materials* **2003**, B103, 247-261.

(13) Marselli, B. Garcia-Gomez, J.; Michaud, P. A.; Rodrigo, M. A.; Comninellis, Ch. Electrogeneration of hydroxyl radicals on boron-doped diamond electrodes. *J. Electrochem. Soc*. **2003**, 150, D79-D83.

(14) Nasr, B.; Abdellatif, G.; Canizares, P.; Saez, C.; Lobato, J.; Rodrigo, M. A. Electrochemical oxidation of hydroquinone, resorcinol, and catechol on boron-doped diamond anodes. *Environ. Sci. Technol*. **2005**, 39, 7234-7239.

(15) Polcar, A. M.; Vacca, A.; Mascia, M.; Palmas, S. Oxidation at boron doped diamond electrodes: an effective method to mineralize triazines. *Electrochim. Acta* **2005**, vol. 50, pages 1841-1847

(16) Caniazres, P.; Diaz, M.; Dominguez, J. A.; Lobato, J.; Rodrigo, M. A. Electrochemical treatment of diluted cyanide aqueous wastes. *J. Chem. Technol. Biotechnol*. **2005**, 80, 565-573.

(17) Bergmann, M. E. H.; Rollin, J. Product and by-product formation in laboratory studies on disinfection electrolysis of water using boron-doped diamond anodes. *Catalysis Today* **2007**, 124, 198-203.

(18) Morao, A.; Lopes, A.; Pessoa de Amorim, M. T.; Groncalves, I. C. Degradation of mixtures of phenols using boron doped diamond electrodes for wastewater treatment. *Electrochim. Acta* **2004**, 49, 1587-1595.

(19) Chailapakul, O.; Popa, E.; Tai, H.; Sarada, B. V.; Tryk, D. A.; Fujishima, A. The electrooxidation of organic acids at boron-doped diamond electrodes. *Electrochem. Comm*. **2000**, 2, 422-426.

(20) Iniesta, J.; Michaud, P. A.; Panizza, M.; Cerisola, G.; Aldaz, A.; Comninellis, Ch. Electrochemical Oxidation of phenol at boron-doped diamond electrode. *Electrochim. Acta* **2001**, 46, 3573-3578.

(21) Scialdone, O.; Galia, A.; Filardo, G. Electrochemical incineration of 1,2-dichloroethane: effect of the electrode material. *Electrochim. Acta* **2008**, 53, 7220-7225.

(22) Menapace, H. M.; Diaz, N.; Weiss, S. Electrochemical treatment of pharmaceutical wastewater by combining anodic oxidation with ozonation. *J. Environ. Sci. and Health Part A* **2008**, 43, 961-968.

(23) Weiss, E.; Groenen-Serraon, K.; Savall, A. A comparison of electrochemical degradation of phenol on boron doped diamond and lead dioxide anodes. *J. Appl. Electrochem*. **2008**, 38. 329-337.

(24) Liao, A. A.; Spitzer, M.; Motheo, A. J.; Bertazzoli, R. Electroombustion of humic acid and removal of algae from aqueous solution. *J. Appl. Electrochem*. **2008**, 38, 721-727.

(25) Scialdone, O.; Galia, G.; Guarisco, C.; Randazzo, S.; Filardo, G. Electrochemical incineration of oxalic acid at boron-doped diamond anodes: role of operative parameters. *Electrochim. Acta* **2008**, 53, 2095-2108.

(26) Pacheco, M. J.; Morao, A.; Lopes, A.; Ciriaco, L.; Goncalves, I. Degradation of phenols using boron-doped diamond electrodes: a method for quantifying the extent of combustion. *Electrochim. Acta* **2007**, 53, 629-636.

(27) Oliveria, R. T. S.; Salazar-Banda, G. R.; Santos, M. C.; Calegaro, M. L.; Miwa, D. W.; Machado, S. A. S.; Avaca, L. A. Electrochemical oxidation of benzene on boron-doped diamond electrodes. *Chemosphere* **2007**, 66, 2152-2158.

(28) Canizares, P.; Garcia-Gomez, J.; Saez, C.; Rodrigo, M. A. Electrochemical oxidation of several chlorophenols on diamond electrodes part I. reaction mechanisms. *J. Appl. Electrochem*. **2003**, 33, 917-927.

(29) Saez, C.; Panizza, M.; Rodrigo, M. A.; Cerisola, G. Electrochemical incineration of dyes using a boron-doped diamond anode. *J. Chem. Technol. Biotechnol*. **2007**, 82, 575-581.

(30) Panizza, M.; Cerisola, G. Electrochemical degradation of methyl red using BDD and PbO2 anodes. *Ind. Eng. Chem. Res*. **2008**, 47, 6816-6820.

(31) Panizza, M.; Cerisola, G. Electrocatalytic materials for the electrochemical oxidation of synthetic dyes. *Appl. Catalysis B: Environ*. **2007**, 75, 95-101.

(32) Martinez-Huitle, C. A.; De Battisti, A.; Ferro, S.; Reyna, S.; Cerro-Lopez, M.; Quiro, M. A. Removal of pesticide methamidophos from aqueous solutions by electrooxidation using Pb/PbO2, Ti/SnO2, and Si/BDD electrodes. *Environ. Sci. Technol*. **2008**, 42, 6929-6935.

(33) Cabeza, A.; Urtiaga, A.; Rivero, M. J.; Ortiz, I. Ammonium removal from landfill leachate by anodic oxidation. *J. Hazard. Materials* **2007**, 144, 715-719.

(34) Organization for Economic Co-operation and Development (OECD). “Results of survey on production and use of PFOS, PFAS, and PFOA, related substances and products/mixtures containing these substances: Environment Directorate Joint Meeting of the Chemicals Committee and the Working Party on Chemicals, Pesticides and Biotechnology, OECD, Paris, January 13, 2005.

(35) Vyas, S. M.; Kania-Korwel, I.; Lehmier, H. J.; Differences in the isomer composition of perfluorooctanesulfonyl (PFOS) derivatives. *J. Environ. Sci. and Health, Part A*. **2007**, 42, 249-255.

(36) Hansen, K. J.; Johnson, H. O.; Eldridge, J. S.; Butenhoff, J. L.; Dick, L. A. Quantitative characterization of trace levels of PFOS and PFOA in the Tennessee River. *Environ. Sci. Technol.* **2002**, 36, 1681-1685.

(37) Taniyasu, S.; Kannan, K.; Horii, Y.; Hanari, N.; Yamashita, N. A survey of perfluorooctane sulfonate and related perfluorinated organic compounds in water, fish, birds, and humans from Japan. *Environ. Sci. Technol.* **2003**, 37, 2634-2639.

(38) So, M. K.; Taniyasu, S.; Yamashita, N.; Giesy, J. P.; Zheng, J.; Fang, Z.; Im, S. H.; Lam, P. K. S. Perfluorinated compounds in costal waters of Hong Kong, South China, and Korea. *Environ. Sci. Technol.* **2004**, 38, 4056-4063.

(39) Boulanger, B.; Peck, A.M.; Schnoor, J. L.; Hornbuckle, K. C. Mass budget of perfluorooctane surfactants in Lake Ontario. *Environ. Sci. Technol*. **2005**, 39, 74-79.

(40) Kannan, K.; Koistinen, J.; Beckmen, K.; Evans, T.; Gorzelany, J. F.; Hansen, K. J.; Jones, P. D.; Helle, E.; Nyman, M.; Giesy, J. P. Accumulation of perfluorooctane sulfonate in marine mammals. *Environ. Sci. Technol*. **2001**, 35, 1593-1598.

(41) Kannan, K.; Franson, J. C.; Bowerman, W. W.; Hansen, K. J.; Jones, P. D.; Giesy, J. P. Perfluorooctane sulfonate in fish-eating water birds including bald eagles and albatrosses. *Environ. Sci. Technol*. **2001**, 35, 3065-3070.

(42) Kannan, K.; Newsted, J.; Halbrook, R. S.; Giesy, J. P. Perfluorooctane sulfonate and related fluorinated hydrocarbons in mink and river otters from the United States. *Environ. Sci. Technol*. **2002**, 36, 2566-2571.

(43) Kannan, K.; Corsolini, S.; Falandysz, J.; Oehme, G.; Focardi, S.; Giesy, J. P. Perfluorinated and related fluorinated hydrocarbons in marine mammals, fishes, and birds from coasts of the Baltic and the Mediterranean Seas. *Environ. Sci. Technol*. **2002**, 36, 3210-3216.

(44) Bossi, R.; Riget, F. F.; Dietz, R. Temporal and spatial trends of perfluorinated compounds in ringed seal (Phoca hispida) from Greenland. *Environ. Sci. Technol.* **2005**, 39, 7416-7422.

(45) Hansen, K. J.; Clemen, L. A.; Ellefson, M. E.; Johnson, H. O. Compound-specific, quantitative characterization of organic fluorochemicals in biological matrices. *Environ. Sci. Technol*. **2001**, 35, 766-770.

(46) Olsen, G. W.; Hansen, K. J.; Stevenson, L. A.; Burris, J. M.; Mandel, J. H. Human donor liver and serum concentrations of perfluorooctane sulfonate and other perfluorochemicals. *Environ. Sci. Technol*. **2003**, 37, 888-891.

(47) Inoue, K.; Okada, F.; Ito, R.; Kato, S.; Saski, S.; Nakajima, S.; Uno, A.; Saijo, Y.; Sata, F.; Yoshimura, Y.; Kishi, R.; Nakazawa, H. Perfluorooctane sulfonate (PFOS) and related perfluorinated compounds in human maternal and cord blood simples: assessment of PFOS exposure in a susceptible population during pregnancy. *Environ. Health Perspect*. **2004**, 112, 1204-1207.

(48) Kannan, K.; Corosolini, S.; Falandysz, J.; Fillmann, G.; Kumar, K. S.; Loganathan, B. G.; Ali Mohd, M.; Olivero, J.; Van Wouwe, N.; Yang, J. H.; Aldous, K. M. Perfluorooctane sulfonate and related fluorochemicals in human blood from several countries. *Environ. Sci. Technol*. **2004**, 38, 4489-4495.

(49) Moriwaki, H.; Takagi, Y.; Tanaka, M.; Tsuruho, K.; Okitsu, K.; Maeda, Y. Sonochemical decomposition of perfluorooctane sulfonate and perfluorooctanoic acid. *Environ. Sci. Technol.* **2005**, 39, 3388-3392.

(50) Schroder, F.; Meesters, R. Stability of fluorinated surfactants in advanced oxidation processes: A follow up of degradation products using flow injection–mass spectrometry, liquid chromatography–mass spectrometry and liquid chromatography–multiple stage mass spectrometry. *J. Chromatography A*. **2005**, 1082, 110-119.

(51) Hori, H.; Hayakawa, E.; Einaga, H.; Kutsuna, S.; Koike, K.; Ibusuki, T.; Kiatagawa, H.; Arakawa, R. Decomposition of environmentally persistent perfluorooctanoic acid in water by photochemical approaches. *Environ. Sci. Technol*. **2004**, 38, 6118-6124.

(52) Hori, H., Nagaoka, Y., Yamamoto, A., Sano, T., Yamashita, N., Taniyasu, S., Kutsuna, S. Efficient decomposition of environmentally persistent perfluorooctanesulfonate and related fluorochemicals using zerovalent iron in subcritical water. *Environ. Sci. Technol*. **2006**, 40, 1049-1054.

(53) Comninellis, Ch. Electrocatalysis in the electrochemical conversion/combustion of organic pollutants for waste water treatment. *Electrochim. Acta* **1994**, 39, 1857-1862.

(54) Gyorgy, F.; Gandini, D.; Comninellis, C.; Perret, A.; Haenni, W. Oxidation of organics by intermediates of water discharge on IrO2 and synthetic diamond anodes. *Electrochem. Solid St.* **1999**, 2, 228-230.

(55) Delley, B. An all-electron numerical-method for solving the local density functional for polyatomic-molecules. *J. Chem. Phys.* **1990**, 92, 508-517.

(56) Delley, B. From molecules to solids with the DMol3 Approach. *J. Chem. Phys.* **2000**, 113, 7756-7764.

(57) Accelrys Corporation, Materials Studio, 4.2, San Diego, CA.

(58) Delley, B. Fast calculation of electrostatics in crystals and large molecules. *J. Phys. Chem.* **1996**, 100, 6107-6110.

(59) Vosko, S. H.; Wilk, L.; Nusair, M. Accurate spin-dependent electron liquid correlation energies for local spin density calculations: a critical analysis. *Can. J. Phys*. **1980**, 58, 1200-1211.

(60) Becke, A. D. A multicenter numerical integration scheme for polyatomic molecules. *J. Chem. Phys*. **1988**, 2547-2553.

(61) Perdew, J. P.; Wang, Y. Accurate and simple analytical representation of the electron-gas correlation energy. *Phys. Rev.* **1992**, B45, 13244-13249.

(62) Delley, B. Hardness conserving semilocal pseudopotentials. *Phys. Rev. B* **2002**, 66, 155125, 1-9.

(*63*) Klamt, A.; Schuurmann, G. COSMO: A new approach to dielectric screening in solvents with explicit expressions for the screening energy and its gradient. *J. Chem. Soc. Perkin Trans. 2* **1993**, 799-805.

(*64*) Halgren, T. A.; Lipscomb, W. N. The synchronous-transit method for determining reaction pathways and locating molecular transition states. *Chem. Phys. Lett*. **1977**, 49, 225-232.

(*65*) Fischer, S.; Karplus, M. Conjugate peak refinement: an algorithm for finding reaction paths and accurate transition states in systems with many degrees of freedom. *Chem. Phys. Lett*. **1992**, 194, 252-261.

(66) Ochterski, J. W. Vibrational analysis in Gaussian. Available at *www.gaussian.com/vib.htm*

(*67*) Hagans, P. L.; Natishan, P. M.; Stoner, B. R.; O'Grady, W. E. Electrochemical oxidation of phenol using boron-doped diamond electrodes. *J. Electrochem. Soc.* **2001**, 148, E298-E301.

(*68*) Tamilmani S.; Huang, W. H.; Raghavan, S.; Farrell, J. Electrochemical treatment of simulated copper CMP wastewater using boron doped diamond thin film electrodes – a feasibility study. *IEEE Transactions of semiconductor manufacturing*. **2004**, 448-454.

(*69*) Farrell, J.; Martin, F. J.; Martin, H. B.; O'Grady, W. E.; Natishan, P. Anodically generated short-lived species on boron-doped diamond film electrodes. *J. Electrochem. Soc.* **2005**, 152, E14-E17.

(*70*) Marselli, B.; Garcia-Gomez, J.; Michaud, P. A.; Rodrigo, M. A.; Comninellis, C. Electrogeneration of hydroxyl radicals on boron-doped diamond electrodes. *J. Electrochem. Soc.* **2003**, 150, D79-D83.

(*71*) Zhu, X.; Shi, S.; Wei, J.; Lv, F.; Zhao, H.; Kong, J.; He, Q. Ni, J. Electrochemical oxidation characteristics of p-substituted phenols using a boron-doped diamond electrode. *Environ. Sci. Technol.* **2007**, 41, 6541-6546.

(72) Smith, J. M. Chemical Engineering Kinetics; McGraw-Hill: New York, 1980.

(73) Murena, F. Schioppa, E.; Gioia, F. Catalytic hydrodechlorination of a PCB dielectric oil. *Environ. Sci. Technol*. **2000**, 34, 4382-4385.

(74) Lin, Y. J.; Chen, Y. L.; Huang, C. Y.; Wu, M. F. Photocatalysis of 2,2',3,4,4',5'-hexachlorobiphenyl and its intermediates using various catalytic preparing methods. *J. Hazard. Mater*. **2006**, 136, 902-910.

(75) Anderson, A. F.; Kang, D. B. Quantum chemical approach to redox reactions including potential dependence: application to a model for hydrogen evolution from diamond. *J. Phys. Chem. A*, **1998**, 102, 5993-5996.

(76) Leach, A. R. Molecular Modeling: Principles and Applications; Prentice Hall: New York, **2001**.

(77) Bockris, J. O'M.; Reddy, A. K. N., Gamboa-Aldeco, M. Modern Electrochemistry, *2nd Ed., Vol. 2A*; Kluwer Academic / Plenum: New York, **2000**.

(*78*) Giesy JP, Kannan K (2001) Environ Sci Technol 35:1339

(79) Kannan, K.; Koistinen, J.; Beckmen, K.; Evans, T.; Gorzelany, J. F.; Hansen, K. J.; Jones, P. D.; Helle, E.; Nyman, M.; Giesy, J. P. Accumulation of perfluorooctane sulfonate in marine mammals. *Environ. Sci. Technol*. **2001**, 35, 1593-1598.

(80) Kannan, K.; Franson, J. C.; Bowerman, W. W.; Hansen, K. J.; Jones, P. D.; Giesy, J. P. Perfluorooctane sulfonate in fish-eating water birds including bald eagles and albatrosses. *Environ. Sci. Technol*. **2001**, 35, 3065-3070.

(81) Hansen, K. J.; Johnson, H. O.; Eldridge, J. S.; Butenhoff, J. L.; Dick, L. A. Quantitative characterization of trace levels of PFOS and PFOA in the Tennessee River. *Environ. Sci. Technol.* **2002**, 36, 1681-1685.

(82) Taniyasu, S.; Kannan, K.; Horii, Y.; Hanari, N.; Yamashita, N. A survey of perfluorooctane sulfonate and related perfluorinated organic compounds in water, fish, birds, and humans from Japan. *Environ. Sci. Technol.* **2003**, 37, 2634-2639.

(83) So, M. K.; Taniyasu, S.; Yamashita, N.; Giesy, J. P.; Zheng, J.; Fang, Z.; Im, S. H.; Lam, P. K. S. Perfluorinated compounds in costal waters of Hong Kong, South China, and Korea. *Environ. Sci. Technol.* **2004**, 38, 4056-4063.

(84) Boulanger, B.; Peck, A.M.; Schnoor, J. L.; Hornbuckle, K. C. Mass budget of perfluorooctane surfactants in Lake Ontario. *Environ. Sci. Technol*. **2005**, 39, 74-79.

(85) Moriwaki, H.; Takagi, Y.; Tanaka, M.; Tsuruho, K.; Okitsu, K.; Maeda, Y. Sonochemical decomposition of perfluorooctane sulfonate and perfluorooctanoic acid. *Environ. Sci. Technol.* **2005**, 39, 3388-3392.

(86) Schroder, F.; Meesters, R. Stability of fluorinated surfactants in advanced oxidation processes: A follow up of degradation products using flow injection–mass spectrometry, liquid chromatography–mass spectrometry and liquid chromatography–multiple stage mass spectrometry. *J. Chromatography A*. **2005**, 1082, 110-119.

(87) Hori, H.; Hayakawa, E.; Einaga, H.; Kutsuna, S.; Koike, K.; Ibusuki, T.; Kiatagawa, H.; Arakawa, R. Decomposition of environmentally persistent perfluorooctanoic acid in water by photochemical approaches. *Environ. Sci. Technol*. **2004**, 38, 6118-6124.

(88) Hori, H., Nagaoka, Y., Yamamoto, A., Sano, T., Yamashita, N., Taniyasu, S., Kutsuna, S. Efficient decomposition of environmentally persistent perfluorooctanesulfonate and related fluorochemicals using zerovalent iron in subcritical water. *Environ. Sci. Technol*. **2006**, 40, 1049-1054.

(*89*) Wade LG Jr (1999) Organic chemistry, 4th edn. Prentice Hall, New York

(90) Boulanger, B.; Vargo. J.; Schnoor, J. L.; Hornbuckle, K. C. Detection of Perfluorooctane Surfactants in Great Lakes Water. *Environ. Sci. Technol*. **2004**, 38, 4064-4070.

(91) Inoue, K.; Okada, F.; Ito, R.; Kato, S.; Sasaki, S.; Nakajima, S.; Uno, A.; Saijo, Y.; Sata, F.; Yoshimura, Y.; Kishi, R.; Nakazawa, H. Perfluorooctane sulfonate (PFOS) and related perfluorinated compounds in human maternal and cord blood samples: assessment of PFOS exposure in a susceptible population during pregnancy. *Environ. Health Perspect*. **2004**, 112, 1204-1207.

(92) Kannan, K.; Newsted, J.; Halbrook, R. S.; Giesy, J. P. Perfluorooctanesulfonate and related fluorinated hydrocarbons in mink and river otters from the United States. *Environ. Sci. Technol*. **2002**, 36, 2566-2571.

(93) Kannan, K.; Franson, J. C.; Bowerman, W. W.; Hansen, K. J.; Jones, P. D.; Giesy, J. P. Perfluorooctane sulfonate in fish-eating water birds including bald eagles and albatrosses. *Environ. Sci. Technol*. **2001**, 35, 3065-3070.

(94) Schroder, F.; Meesters, R. Stability of fluorinated surfactants in advanced oxidation processes: A follow up of degradation products using flow injection–mass spectrometry, liquid chromatography–mass spectrometry and liquid chromatography–multiple stage mass spectrometry. *J. Chromatography A*. **2005**, 1082, 110-119.

(95) Lau, C.; Butenhoff, J. L.; Rogers, J. M. The developmental toxicity of perfluoroalkyl acids and their derivatives. *Toxicol. Applied Pharm*. **2004**, 198, 231-241.

(96) Boss. R.; Riget, F. F.; Dietz, R. Temporal and spatial trends of perfluorinated compounds in ringed seal (phoca hispida) from Greenland. *Environ. Sci. Technol*. **2005**, 39, 7416-7422.

(97) Ellis, D.A.; Mabury, S. A.; Martin, J. W.; Muir, D. C. G. Thermolysis of fluoropolymers as a potential source of halogenated orgainic acids in the environment. *Nature* **2001**, 412, 321-324.

(98) Hori, H.; Hayakawa, E.; Einaga, H.; Kutsuna, S.; Koike, K.; Ibusuki, T.; Kiatagawa, H.; Arakawa, R. Decomposition of environmentally persistent perfluorooctanoic acid in water by photochemical approaches. *Environ. Sci. Technol.* **2004**, 38, 6118-6124.

(99) Yamamoto, T.; Noma, Y.; Sakai, S. I.; Shibata, Y. Photodegradation of perfluorooctane sulfonate by UV irradiation in wter and alkaline 2-propanol. *Environ. Sci. Technol*. **2007**, 41, 5660-5665.

(100) Moriwaki, H.; Takagi, Y.; Tanaka, M.; Tsuruho, K.; Okitsu, K.; Maeda, Y. Sonochemical decomposition of perfluorooctane sulfonate and perfluorooctanoic acid. *Environ. Sci. Technol.* **2005**, 39, 3388-3392.

(101) Hori, H.; Nagaoka, Y.; Yamamoto, A.; Sano, T.; Yamashita, N.; Taniyasu, S.; Kutsuna, S. Efficient decomposition of environmentally persistent perfluorooctanesulfonate and related fluorochemicals using zerovalent iron in subcritical water. *Environ. Sci. Technol.* **2006**, 40, 1049-1054.

(102) Ochoa-Herrera, V.; Sierra, R.; Somogyi, A.; Jacobsen, N. E.; Wysocki, V. H.; Field, J. A. Reductive defluorination of perfluorooctane sulfonate. *Environ. Sci. Technol*. **2008**, 42, 3260-3264.

(103) Carter, K. E.; Farrell, J. Oxidative destruction of perfluorooctane sulfonate using boron-doped diamond film electrodes. *Environ. Sci. Technol*. **2008**, 42, 6111-6115.

(104) Tang, C. Y.; Fu, Q. S.; Criddle, C. S.; Leckie, J. O. Effect of flux (transmembrane pressure) and membrane properties on fouling and rejection of reverse osmosis and nanofiltration membranes treating perfluorooctane sulfonate containing wastewater. *Environ. Sci. Technol*. **2007**, 41, 2008-2014.

(105) Ochoa, V.; Sierra, R. Removal of perfluorinated surfactants by sorption onto granular activated carbon, zeolite, and sludge. *Chemosphere* **2008**, 72, 1588-1593.

(106) Lampert, D. J.; Frish, M. A.; Speitel, G. E. Removal of perfluorooctanoic acid and perfluorooctane sulfonate from wastewater by ion exchange. *Pract. Period. Hazard. Toxic. Radioact. Waste Manage*. **2007**, 60-68.

(107) Ihara, Y. Adsorption of anionic surfactants and related compounds from aqueous solution onto activated carbon and synthetic adsorbent. *J. Appl. Poly. Sci*. **1992**, 44, 1837-1840.

(108) Chen, X.; Farber, M.; Gao, Yuming; Kulaots, I.; Suuberg, E. M.; Hurt, R. H. Mechanisms of surfactant adsorption on non-polar, air-oxidized and ozone-treated carbon surfaces. *Carbon* **2003**, 41, 1489-1500.

(109) Ruthven, D. M. Principles of Adsorption and Adsorption Processes. Wiley-Interscience Publication, New York, 1984.

(110) Wu, S. H.; Pendleton, P. Adsorption of anionic surfactant by activated carbon: effect of surface chemistry, ionic strength, and hydrophobicity. *J. Colloid and Interface Sci.* **2001**, 243, 306-315.

(111) Schwarzenbach, R. P.; Gschwend, P. M.; Imboden, D. M. Environmental Organic Chemistry. Wiley Interscience Publication, New York, 1993.

(112) Boudreau, T. M.; Sibley, P. K.; Mabury, S. A.; Muir, D. G. C.; Solomon, K. R. Laboratory evaluation of the toxicity of perfluorooctane sulfonate (PFOS) on selenastrum capricornutum, chlorella vulgaris, lemna gibba, daphnia, magna, and daphnia pulicaria. *Arch. Environ. Contam. Toxicol*. **2003**, 44, 307-313.

(113) Beach, S. A.; Newsted, J. L.; Coady, K.; Giesy, J. P. Ecotoxicological evaluation of perfluorooctanesulfonate (PFOS). *Rev. Environ. Contam. Toxicol*. **2006**, 186, 133-174.

(114) Chung, J.; Krajmalnik-Brown, R.; Rittmann, B. E. Bioreduction of trichloroethene using a hydrogen-based membrane biofilm reactor. *Environ. Sci. Technol*. **2008**, 42, 477-483.

(115) Chen, G.; Betterton, E. A., Arnold, R. G. Electrolytic oxidation of trichloroethylene using a ceramic anode. *J. Appl. Electrochem*. **1999**, 29, 961-970.

(116) Ellis, D. E.; Lutz, E. J.; Odom, J. M.; Bartlett, C. L.; Lee, M. D.; Harkness, M. R.; Deweerd, K. A. Bioaugmentation for accelerated in situ anaerobic bioremediation. *Environ. Sci. Technol*. **2000**, 34, 2254-2260.

(117) Sunder, M.; Hempel, D. C. Oxidation of Tri- and Perchloroethene in aqueous solution with ozone and hydrogen peroxide in a tube reactor. *Wat. Res*. **1997**, 31, 33-40.

(118) Pelech, R.; Milchert, E.; Bartkowiak, M. Fixed-bed adsorption of chlorinated hydrocarbons from multicomponent aqueous solution onto activated carbon: equilibrium column model. *J. Coll. Inter. Sci*. **2006**, 296, 458-464.

(119) Browne, T. E.; Cohen, Y. Aqueous-phase adsorption of trichloroethene and chloroform onto polymeric resins and activated carbon. *Ind. Eng. Chem. Res*. **1990**, 29, 1338-1345.

(120) Miranda, B.; Diaz, E.; Ordonez, S.; Vega, A. Diez, F. V. Oxidation of trichloroethene over metal oxide catalysts: kinetic studies and correlation with adsorption properties. *Chemosphere* **2007**, 66, 1706-1715.

(121) Miranda, B.; Diaz, E.; Ordonez, S.; Vega, A. Diez, F. V. Performance of alumina-supported noble metal catalysts for the combustion of trichloroethene at dry and wet conditions. *Appl. Catal. B: Environ*. **2006**, 64, 262-271.

(122) Miranda, B.; Diaz, E.; Ordonez, S.; Vega, A. Diez, F. V. Catalytic combustion of trichloroethene over Ru/Al2O3: reaction mechanism and kinetic study. *Catal. Commun*. **2006**, 7, 945-949.

(123) Li, K.; Stefan, M. I.; Crittenden, J. C. Trichloroethene degradation by UV/H2O2 advanced oxidation process: product study and kinetic modeling. *Environ. Sci. Technol*. **2007**, 41, 1696-1703.

(124) Hirvonen, A.; Tuhkanen, T.; Kalliokoski, P. Treatment of TCE and PCE-contaminated groundwater using UV/H2O2 and O3/H2O2 oxidation processes. *Water Sci. Technol*. **1996**, 33, 67.

(125) Weir, B. A.; McLane, C.R.; Leger, R. J. Design of a UV oxidation system for treatment of TCE-contaminated groundwater. *Environ. Prog*. **1996**, 15, 179-186.

(126) Weir, B. A.; Sundstrom, D. W. Destruction of trichloroethylene by UV light-catalyzed oxidation with hydrogen peroxide. *Chemosphere* **1993**, 27, 1279-1291.

(127) Glaze, W. H.; Kang, J. W. Advanced oxidation processes for treating groundwater contaminated with TCE and PCE: Laboratory studies. Journal of American Water Works Association, 1998.

(128) Knauss, K. G.; Dibley, M. J.; Leif, R. N.; Mew, D. A.; Aines, R. D. Aqueous oxidation of trichloroethene (TCE): a kinetic analysis. Appl. Geochem. 1999, 14, 531-541.

(129) De Visscher, A.; Van Langenhove, H. Sonochemistry of organic compounds in homogeneous oxidizing systems. Ultrasonic Sonochemistry, 1998, 5, 87-92.

(130) Drijvers, D.; De Baets, R.; Visscher, A. D.; Van Langenhove, H. Sonolysis of trichloroethylene in aqueous solution: volatile organic intermediates. Ultrasonic Sonochem. 1996, 3, S83-S90.

(131) Shen, Y. S.; Ku Y. Decomposition of gas-phase trichloroethene by the UV/TiO2 process in the presence of ozone. *Chemosphere* **2002**, 46, 101-107.

(132) Kao, C. M.; Huang, K. D.; Wang, J. Y.; Chen, T. Y.; Chien, H. Y. Application of potassium permanganate as an oxidant for in situ oxidation of trichloroethylene – contaminated groundwater: a laboratory and kinetics study. J. Hazard. Mater. 2008, 153, 919-927.

(133) Liang, C.; Bruell, C. J.; Marley, M. C.; Sperry, K. L. Persulfate oxidation for in situ remediation of TCE I: Activated by ferrous iron with and without persulfate-thiosulfate redox couple. Chemosphere, 2004, 55, 1213-1223.

(134)Liang, C.; Bruell, C. J.; Marley, M. C.; Sperry, K. L. Persulfate oxidation for in situ remediation of TCE II: Activated by chelated ferrous iron. Chemosphere, 2004, 55, 1225-1233.

(135) Lee, E. S.; Soel, Y.; Fang, Y. C.; Schwartz, F. W. Destruction efficiencies and dynamics of reaction fronts associated with the permanganate oxidation of trichloroethylene. Environ. Sci. Technol. 2003, 37, 2540-2546.

(136) Yan, Y. E.; Schwartz, F. W. Oxidative degradation and kinetics of chlorinated ethylenes by potassium permanganate. J. Contam. Hydrology. 1998, 37, 343-365.

(137) Waldemer, R. H.; Tratnyek, P. G.; Johnson, R. L.; Nurmi, J. T. Oxidation of chlorinated ethenes by heat-activated persulfate: kinetics and products. Environ. *Sci. Technol*. **2007**, 41, 1010-1015.

(138) Li, T.; Farrell, J. Reductive dechlorination of trichloroethene and carbon tetrachloride using iron and palladized-iron cathodes. *Environ. Sci. Tech*. **2000**, 34, 173-179.

(139) Petersen, M. A.; Sale, T. C.; Reardon, K. F. Electrolytic trichloroethene degradation using mixed metal oxide coated titanium mesh electrodes. *Chemosphere* **2007**, 67, 1573-1581.

(140) Mishra, D.; Liao, Z.; Farrell, J. Understanding reductive dechlorination of trichloroethene on boron-doped diamond film electrodes. Environ. Sci. Technol. 2008, 42, 9344-9349.

(141) Foti, G.; Gandini, D. J.; Comninellis, C.; Perret, A.; Haenni, W. Oxidation of organics by intermediates of water discharge on IrO2 and synthetic diamond anodes. Electrochem. Solid-State Lett. 1999, 2, 228-230.

(142) Comninellis, C.; Nerini, A. Anodic oxidation of phenol in the presence of NaCl for wastewater treatment. J. Appl. Electrochem. 1995, 25, 23-29.

(143) Perret, A. J.; Haenni, W.; Skinner, N.; Tang, X. M.; Gandini, D.; Comninellis, C.; Correa, B.; Foti, G. Electrochemical behavior of synthetic diamond thin film electrodes. Diamond Relat. Mater. 1998, 8, 820-823.

(144) Gherardini, L.; Michaud, P. A.; Panizza, M.; Comninellis, C. Vatistas, N. Electrochemical oxidation of 4-chlorophenol for wastewater treatment. J. Electrochem. Soc. 2001, 148, D78-D82.

(145) Hagans, P. L.; Natishan, P. M.; Stoner, B. R.; O'Grady, W. E. Electrochemical oxidation of phenol using boron doped diamond electrodes. J. Electrochem. Soc. 2001, 148, E298-E301.

(146) Iniesta, J.; Michaud, P. A.; Panizza, M.; Cerisola, G.; Aldaz, A.; Comninellis, C. Electrochemical oxidation of phenol at boron diamond film electrode. Electrochim. Acta 2001, 46, 3573-3578.

(147) Delley, B. An all-electron numerical-method for solving the local density functional for polyatomic-molecules. *J. Chem. Phys.* **1990**, 92, 508-517.

(148) Delley, B. From molecules to solids with the DMol3 Approach *J. Chem. Phys.* **2000**, 113, 7756-7764.

(149) Accelrys Corporation, Materials Studio, 4.2, San Diego, CA.

(150) Delley, B. Fast calculation of electrostatics in crystals and large molecules. *J. Phys. Chem.* **1996**, 100, 6107-6110.

(*151*) Becke, A. D. Density-functional exchange-energy approximation with correct asymptotic behavior. *Phys. Rev. A* **1988**, 38, 3098-3100.

(*152*) Lee C.; Yang W.; Parr, R.G. Development of the Colle-Salvetti correlation-energy formula into a functional of the electron density. *Phys. Rev. B* **1988**, 37, 785-789.

(153) Delley, B. Hardness conserving semilocal pseudopotentials. *Phys. Rev. B* **2002**, 66, 155125, 1-9.

(*154*) Delley, B., The conductor-like screening model for polymers and surfaces. *Mol. Simulat.* **2006**, 32, 117-123.

(*155*) Halgren, T. A.; Lipscomb, W. N. The synchronous-transit method for determining reaction pathways and locating molecular transition states. *Chem. Phys. Lett*. **1977**, 49, 225-232.

(*156*) Fischer, S.; Karplus, M. Conjugate peak refinement: An algorithm for finding reaction paths and accurate transition states in systems with many degrees of freedom. *Chem. Phys. Lett*. **1992**, 194, 252-261.

(157) Barbosa, L. A. M. M.; Sautet, P. Trichloroethene dechlorination reaction on the PdCu (110) alloy surface: A periodical density functional theory study of the mechanism. *J. Catal.* **2002**, 207, 127-138.

(158) Ochterski, J. W. Vibrational analysis in Gaussian. *www.gaussian.com/vib.htm*

(159) Anderson, A. F.; Kang, D. B. Quantum chemical approach to redox reactions including potential dependence: application to a model for hydrogen evolution from diamond. *J. Phys. Chem. A*, **1998**, 102, 5993-5996.

(160) Bockris, J. O'M.; Reddy, A. K. N., Gamboa-Aldeco, M. Modern Electrochemistry, *2nd Ed., Vol. 2A*; Kluwer Academic / Plenum: New York, **2000**.